Developing Connections for Longitudinal Joints between Deck Bulb Tees — Development of UHPC Mixes with Local Materials

WA-RD 869.1

Pizhong Qiao
Zhidong Zhou
Srinivas Allena

October 2016

Washington State Department of Transportation
Office of Research & Library Services

WSDOT Research Report

17-10-0413

Final Report

Agreement T1462, Task 6

WA-RD 869.1

DEVELOPING CONNECTIONS FOR LONGITUDINAL JOINTS BETWEEN DECK BULB TEES - DEVELOPMENT OF UHPC MIXES WITH LOCAL MATERIALS

(In collaboration with Prof. John Stanton, University of Washington)

by

Pizhong Qiao, Ph.D., P.E.
Professor, WSU

Zhidong Zhou, Ph.D. Student
Research Assistant, WSU

Srinivas Allena, Ph.D., P.E.
Clinical Assistant Professor, WSU

Washington State Transportation Center (TRAC)
Washington State University
Department of Civil and Environmental Engineering
Sloan Hall, Room 101
Pullman, WA 99164-2910

Washington State Department of Transportation

Lu Saechao, P.E.
Research Manager

Bijan Khaleghi, Ph.D., P.E., State Bridge Design Engineer
Technical Contact

Prepared for

The State of Washington
Washington State Department of Transportation
Roger Millar, Secretary

October 2016

1. REPORT NO.	2. GOVERNMENT ACCESSION NO.	3. RECIPIENT'S CATALOG NO.
WA-RD 869.1		

4. TITLE AND SUBTITLE	5. REPORT DATE
Developing Connections for Longitudinal Joints between Deck Bulb Tees - Development of UHPC Mixes with Local Materials	October 2016
	6. PERFORMING ORGANIZATION CODE
7. AUTHOR(S)	8. PERFORMING ORGANIZATION REPORT NO.
Pizhong Qiao, Zhidong Zhou and Srinivas Allena	
9. PERFORMING ORGANIZATION NAME AND ADDRESS	10. WORK UNIT NO.
Washington State Transportation Center (TRAC) Washington State University Department of Civil and Environmental Engineering Pullman, WA 99164-2910	11. CONTRACT OR GRANT NO. Agreement T1462, Task 6
12. SPONSORING AGENCY NAME AND ADDRESS	13. TYPE OF REPORT AND PERIOD COVERED
Washington State Department of Transportation Transportation Building, MS: 47372 Olympia, WA 98504-7372 Research Manager: Lu Saechao by 360.705.7260	Final Report
	14. SPONSORING AGENCY CODE

15. SUPPLEMENTARY NOTES

This study was conducted in cooperation with the U.S. Department of Transportation, Federal Highway Administration

16. ABSTRACT

In past decades, many state DOTs and the Federal Highway Administration (FHWA) have begun working with ultra-high performance concrete (UHPC), an advanced cementitious material. The Washington State Department of Transportation (WSDOT) has not employed the UHPC in highway bridge applications, such as connection joints for precast concrete decks and girders due to its high cost and lack of experience. In this study, two viable mixtures (A4 and C3) were selected from an array of trial UHPC mixtures produced using local materials (primarily the local fine sand and domestic steel fiber) for extensive performance evaluation. The physical and mechanical properties (including workability, compressive and tensile strength, elastic modulus, and shrinkage) of selected UHPC mixtures and their bond properties with the epoxy-coated reinforcing bars were investigated.

The two considered mix designs exhibited compressive strength up to 16 ksi, direct tensile strength of 1.1 ksi, elastic modulus of 5,000 ksi, and relatively high bond strength. Shrinkage was also characterized and found to be about 600 με which is comparable to that of conventional concrete. Based on the comparisons of material properties and bond strength of two selected mixtures, the mixture C3 outperforms the mixture A4, and it is thus recommended to be used in the second phase of the project study for the structural level testing and evaluation at the University of Washington.

17. KEY WORDS	18. DISTRIBUTION STATEMENT
Ultra-High Performance Concrete (UHPC), Connection Joints, Mix Design, Mechanical Characterization, Tensile Behavior, Pull-out Behavior	No restrictions. This document is available to the public through the National Technical Information Service, Springfield, VA 22616

19. SECURITY CLASSIF. (of this report)	20. SECURITY CLASSIF. (of this page)	21. NO. OF PAGES	22. PRICE
Unclassified	Unclassified		

DISCLAIMER

The contents of this report reflect the views of the authors, who are responsible for the facts and accuracy of the data presented herein. The contents do not necessarily reflect the official views or policies of the Washington State Department of Transportation or the Federal Highway Administration. This report does not constitute a standard, specification, or regulation.

ACKNOWLEDGEMENTS

The authors thank Professor John Stanton of the University of Washington, Dr. Bijan Khaleghi and engineers in Bridge & Structures Office of WSDOT, and Lu Saechao of WSDOT for their technical input and support. The materials provided by the BASF Corporation are gratefully acknowledged.

TABLE OF CONTENTS

LIST OF TABLES

Page

LIST OF FIGURES

EXECUTIVE SUMMARY

Precast decked members, such as deck bulb tees, are presently not used by the Washington State Department of Transportation (WSDOT) on major highways, largely because bridges built with them on fewer numbers of roads have shown cracks along the longitudinal joints. The connections in those bridges used a combination of welded clips and a grouted joint. Some state DOTs and the Federal Highway Administration (FHWA) have recently researched and/or implemented other connection approaches. These include narrow cast-in-place joints, ultra-high performance concrete (UHPC) for such joints, headed bars to achieve development within the width of the joint, and various combinations thereof. The primary drawbacks of these connection approaches are: UHPC is expensive, proprietary and enjoys little field expertise outside Ductal; headed bars may pose interference problems during erection and possible cover violations if camber is not well-controlled; narrow joints (desirable if expensive materials are used to fill them) could reduce the available development length below an acceptable level if the precast member has significant sweep. An ideal solution has yet to be found.

The goal of the research is to develop a UHPC mixture using materials available locally and domestically as an alternative to commercially available pre-packaged UHPC products. Selection of these local materials not only reduces the cost of UHPC but also improve the sustainability. In the subsequent study, the recommended UHPC mixture will be investigated at the University of Washington in the connection joints for stiffness and strength in bending.

In this study, several trial UHPC mixtures produced with locally available cement, sand, and admixtures as well as domestic steel fibers were evaluated, from which two

viable UHPC mixtures were selected for further investigation. More importantly, the expensive materials, such as quartz powder and imported fibers, commonly used in commercial products and other studies, were not used in this study. The mechanical properties of selected UHPC mixtures and their bond properties with the epoxy-coated reinforcing bars were investigated, from which one final UHPC mix design was recommended for application in the joint connections of intended bridge deck bulb tees.

1) Based on the experimental evaluation of UHPC mixtures produced, the following findings/conclusions are drawn: (1) The proper mixing procedures of UHPC are recommended, and the aim is to achieve adequate workability of mixtures with thorough mixing time. (2) Following the standard test procedures for concrete and cementitious material characterization, the test methods for both the fresh and harden properties of UHPC are selected, and the pull-out strength tests of concrete are adopted for characterization of bond strength of reinforcing bars in UHPC. The tensile strength-related properties and test methods of UHPC are emphasized. (3) The standard test method for flow of hydraulic cement mortar (ASTM C1437) (the flow test) was considered to evaluate the rheology of UHPC. The flow tests were conducted on all 12 trial UHPC mixtures. The final two UHPC mixtures (A4 and C3) exhibited a spread of 9 inches, which is considered in practice as the minimum required for bridge deck applications. (4) The compressive strength of UHPC was evaluated using 2 inch and 4 inch cube specimens (ASTM C109). The 2 inch cube specimens exhibited greater compressive strengths than the 4 inch cubes, and the specimens produced from mixture C3 exhibited a slightly greater compressive strength than mixture A4. It was also observed that the maximum potential of compressive strength almost reached after 14 days. (5) The flexural strength (modulus of rupture)

(ASTM C78), splitting tensile strength (ASTM C496), and the direct tension tests were conducted to evaluate the tensile strength-associated properties. The direct tension test produced the lowest tensile strength values, followed by the splitting tensile strength test, and then the flexural strength test. The direct tension test using the dog-bone shaped samples is regarded as the most accurate method to obtain the tensile strength properties. More than 80% of the full tensile strength is achieved after 7 days, and the tensile strength of mixture C3 is about 30.8% greater than that of mixture A4 based on the direct tension test. Besides obtaining the tensile strength of the materials, the direct tension test is also capable of measuring the whole stress-strain curves of the samples, from which the constitutive behavior and ductility of UHPC materials are characterized. (6) Both the autogenous and free shrinkage properties were measured using two different sizes of prismatic specimens (4 x 4 x 11.25 inch and 1 x 1 x 11.25 inch) (ASTM C157). The 1 x 1 x 11.25 inch prismatic samples shrank more than the 4" x 4 x 11.25 inch prismatic ones. The autogenous shrinkage and free shrinkage values of 4 x 4 x 11.25 inch prisms are almost equal for mixtures A4 and C3. The restrained shrinkage test was performed as well using the AASHTO ring, and mixture C3 exhibited smaller restrained shrinkage values than that of mixture A4. (7) UHPC shows excellent freeze-thaw resistance as well as negligible surface scaling under frost action. (8) The pull-out test was conducted to evaluate the bond strength of epoxy-coated reinforcing steel bar in UHPC. Side cover and embedment length were also investigated using a No. 5 epoxy-coated rebar of Grade 60 and bar spacing of 7 inch. The majority of the pull-out specimens failed in splitting. For the bar with a longer embedment length, the yielding of the rebar was observed. Mixtures A4 and C3 result in comparably the same bond strength.

Based on the mixture development and experimental program performed in this study, the following recommendations are suggested to further improve the mix design and better understand the performance of UHPC: (1) In the present study, sand was sieved through ASTM No. 30 and No. 200 sieves to obtain the particle size range between 75-600 microns. Since the scalping of sand is extremely time- and labor-consuming, studies need to be conducted to understand the effect of nominal maximum size of particle on rheological, physical, and mechanical properties of UHPC. (2) Optimization of particle packing density is important to achieve greater mechanical strength of UHPC. Studies to determine particle packing of granular mixture that can help achieve workable mixes and superior mechanical behavior of UHPC needs to be conducted. (3) UHPC mixtures developed in this study should be further optimized with w/cm ratios lower than 0.14. UHPC mixtures produced with much lower w/cm ratios are expected to exhibit greater mechanical strength and superior durability characteristics. (4) Utilize high levels of industrial wastes, such as GGBFS and fly ash, to partially replace silica fume and cement and thus produce economical and eco-friendly UHPC. (5) The properties, such as compressive strength, tensile strength and durability, are directly dependent on curing and post setting heat treatment methods. Further study is recommended to investigate the effect of different curing regimens on the properties of UHPC and identify a practically feasible curing regimen. (6) Although it was established that UHPC exhibits superior resistance to rapid freeze-thaw resistance, freeze-thaw behavior of UHPC when exposed harsh environments and cold climates, such as marine environment, chlorine deicer coupled with freeze-thaw cycles, magnesium deicer coupled with freeze-thaw cycles, etc., should also be investigated in Washington State. (7) Both early-age and long-term shrinkage and creep performance

due to loss of moisture and the shrinkage cracking tendency on the concrete surface with a risk of decreasing the quality and durability need to be fully understood as UHPC has a very low water/cementitious materials ratio. Additionally, potential mitigation strategies, such as using shrinkage reducing admixtures (SRA), expansive cementitious materials, and internal curing, etc., can be proposed to reduce the shrinkage cracking tendency. (8) In this study, due to the short gage length of extensometer, some cracks occurred out of its range, and a modified testing method is needed to capture the ductile post-cracking behavior of UHPC in direct tension. (9) Extended pull-out (bond strength) tests regarding more design parameters (e.g., bar spacing, bar size, and bar types, etc.), loading regimes (e.g., biaxial loading, triaxial loading, etc.), and age of UHPC, etc., are recommended to understand the bond behaviors. (10) Other behaviors of UHPC when subjected to fatigue and dynamic impact loadings are also needed to ensure structural applications in bridge engineering.

In summary, the mix design of UHPC with locally available materials and related mechanical properties tests are conducted. Based on the comparisons of material properties and bond strength of two selected mixtures (i.e., A4 and C3), the mixture C3 outperforms the mixture A4, and it is thus recommended to be used in the second phase of the project study for the structural level testing and evaluation at the University of Washington.

Chapter 1 INTRODUCTION

1.1 Problem Statement

Precast decked members, such as deck bulb tees, are presently not used by the Washington State Department of Transportation (WSDOT) on major highways, largely because bridges built with them on minor roads have shown cracks along the longitudinal joints. The connections in those bridges used a combination of welded clips and a grouted joint. Some state DOTs and the Federal Highway Administration (FHWA) have recently researched and/or implemented other connection approaches which include narrow cast-in-place joints, ultra-high performance concrete (UHPC) for such joints, headed bars to achieve development within the width of the joint, and various combinations thereof. The primary drawbacks include: UHPC is expensive, proprietary and little field expertise outside Ductal; headed bars may pose interference problems during erection and possible cover violations if camber is not well-controlled; narrow joints (desirable if expensive materials are used to fill them) could reduce the available development length below an acceptable level if the precast member has significant sweep. An ideal solution has yet to be found.

The goal of the research is to develop a UHPC mixture using locally and/or domestically available materials, thereby avoiding the high costs of the proprietary material. In the subsequent study, the developed UHPC mixture will be investigated at the University of Washington (UW) in the connection joints for stiffness and strength in bending.

1.2 Research Objectives

The goal of the work is two-fold: (1) to develop UHPC mixtures, as much as possibly

with locally available materials, for use in the joints, and (2) to establish its critical properties, particularly the tensile strength of UHPC and bond behaviors. The following activities are performed in this study:

1 - Literature Review and Identification of Local Materials

Conduct a literature review and contact others with experience in UHPC to develop a starting point for a suitable mixture. Identify locally sourced materials suitable for UHPC mixture development.

2 - Development of Trial Mixtures

Develop trial mixtures. Criteria will include high bond strength, high tension strength, and good working properties (e.g., workability, low shrinkage, low permeability, high durability, etc.). These properties are the primary ones needed for a successful connection. Very high compressive strength may not be essential if these other properties suitable for developing good joint connections can be obtained.

3 - Material Property Tests

Conduct material property tests (e.g., strength, stiffness, shrinkage, permeability, etc.) on the trial mixtures.

4 - Bond Pullout Tests

Conduct bond capacity tests using pullout specimens with a range of embedded lengths, spacing, and cover. These will be conducted on No. 5 G60 epoxy-coated bars. The goal is to determine the lengths of embedment in UHPC needed to develop yielding in the bars and fracture in UHPC.

5 - Collaboration with UW for Joint Development with UHPC

Provide UHPC mix design and oversight for casting the joints in deck joint specimens

to be constructed and tested in the lab at UW.

6 - Data Analysis and Reporting

Conduct data analysis and report the findings from this study.

Chapter 2 LITERATURE REVIEW

This chapter focuses on the past studies, which have been conducted regarding development of UHPC and evaluation of its properties. The constituents of UHPC, the strength and durability related properties, with emphasis on various specimen sizes and innovative testing methods, and the importance of UHPC in terms of its potential for application in the bridge industry have been discussed in detail.

2.1 Materials and Production of UHPC

2.1.1 Constituent materials

The constituents of the UHPC are not totally different from those of the conventional concrete. However, some additional constituents, such as ground quartz, silica fume, steel aggregates, high range water reducing admixtures (HRWRA), steel fibers, and very high cement content, are considered in producing UHPC mixtures. The premix of UHPC is being manufactured by some companies around the world, among which are Ductal for North America construction industry, and the composition of such mix is given in Table 2.1 (Graybeal, 2006).

Comparing the percentage of water to the cementitious materials in Table 2.1, it can be seen that there is very little water present for the hydration process. Thus, UHPC mix has low water-cement ratio (w/c) of 0.20 and low water-cementitious materials ratio (w/cm) of 0.15. Use of HRWRA allows implementing such a very low w/cm ratio in UHPC mixtures with desired workability, thus ensuring self-compacting concrete to be produced. Since it is not all the cement particles that can participate in the hydration process because of low w/cm, the un-hydrated cement particles act as aggregate in the mix. It should be

noted from Table 2.1 that there is no coarse aggregate in UHPC mix, so UHPC is treated as a homogeneous material. Fine sand with diameter less than 0.6 mm is widely used in UHPC to achieve better performance, because there is low porosity and low permeability in UHPC (Graybeal, 2006; Allena and Newtson, 2011). Fine sand with maximum sizes of 0.8 mm and 1.2 mm was also considered by Collepardi et al. (1997) and Li et al. (2009), respectively, and no significant change occurred on the compressive strength of UHPC when small amount of coarse sand was contained. Some other researchers also used coarse aggregates (such as crushing basalt, natural sand, and limestone) up to 12.7 mm to partially replace fine sand, and they obtained comparable or lower compressive strength but lower flexural and bond strength. It has been found that porosity increases with the increasing content of coarse aggregates (Reda et al., 1999; Zhao et al., 2014; Wille and Boisvert-Cotulio, 2015; Liu et al, 2016; Sobuz et al., 2016). Steel fibers are present in UHPC mix to assist in increasing its tensile strength and invariably increasing its ductility. However, reinforcement bars (rebars) are not required when using UHPC. The 2% per volume of straight steel fibers were used in the mix as recommended by the commercial manufacturer Ductal to product economical and workable UHPC mixtures (Graybeal, 2006; Richard and Cheyrezy, 1995). Wille et al. (2011) explained that this specified volume fraction provides a good compromise between cost, reinforcement, ductility and workability. In comparison to twisted-end and hooked-end steel fibers, straight fibers exhibit lower strain hardening but more strain softening behaviors (Park et al., 2012). In UHPC in cooperation with straight fibers, no suddenly lose strength occurs when post crack initials, because straight fibers are gradually pulled out form the cement matrix. In UHPC with twisted-end and hooked-end fibers, the fracture of cement matrix resulted in less ductile behavior.

Table 2.1 The composition of Ductal UHPC mix (Graybeal, 2006)

Material	Amount (kg/m^3 [lb/yd^3])	Percent per weight (%)
Portland Cement	712 (1,200)	28.5
Fine Sand	1,020 (1,720)	40.8
Silica Fume	231 (390)	9.3
Ground Quartz	211 (355)	8.4
Superplasticizer (HRWRA)	30.7 (51.8)	1.2
Accelerator	30 (50.5)	1.2
Steel Fibers	156 (263)	6.2
Water	109 (184)	4.4

The mixture proportion of UHPC greatly affects the desired mechanical properties in the sense that it dictates if the high compressive strength and high durability associated with UHPC will be achieved or not. Researchers have worked on making sure that UHPC brings out the required properties as expected, and among them are Graybeal (2006), Li et al. (2009), Allena and Newtson (2011), Cornelia et al. (2012), and Hassan and Jones (2012). Tables 2.1, 2.2, 2.3, 2.4, and 2.5 show the different UHPC mix proportions developed by these researchers, respectively.

The constituents used for the UHPC mix in Table 2.3 were all locally produced apart from the silica fume. The cement used was the high-strength Portland cement CEM I 52.5R. The silica fume has a high SiO_2 content. The HRWRA used was Glenium ACE440 produced by BASF Romania. In addition, two types of high strength fibers were used: 50% long hooked end fibers (WMS-25/0.4/4/304) with L/d = 25/0.4, and 50% short straight fibers (MSF-6/0.175/5-26WB) with L/d=15/0.2, with the minimum tensile strength of 1,450 MPa and 2,200 MPa, respectively. The fibers were produced by Baumbach Metall Gmbh - Germany. The fiber density was 7.85 g/cm^3. 2.55 % per volume of these steel fibers

were used in the mix.

Table 2.2 UHPC mix proportions (kg/m^3) (Allena and Newtson, 2011)

Category	A	B		C		D	E
Cement	940	710	852	890	1,067	890	890
Silica Fume	-	230	276	222	267	222	222
Fine Sand	924	844	535	793	498	837	799
Steel Fiber	190	190	189	-	-	-	119
Water	263	263	315	245	294	222	222
HRWRA (l/ m^3)	23.5	14.8	16.0	24.7	17.3	29.6	29.6
w/c	0.28	0.37	0.37	0.275	0.275	0.25	0.25
w/cm	0.28	0.28	0.28	0.22	0.20	0.20	0.20

Table 2.3 UHPC mix proportions per weight (Cornelia et al., 2012)

Test type	OE23	ME23
Portland Cement	1	1
Silica Fume	0.259	0.259
Quartz Sand	0.61	0.69
Steel Fiber	0.19	-
HRWRA	0.065	0.065
w/cm	0.129	0.125

Note: OE23 - with steel fiber; ME23 - without steel fiber

Table 2.4 UHPC mix proportions by weight (Li et al., 2009)

Constituents	Product/Manufacturer	Proportion by weight of concrete (kg/m^3)
Premix	Ductal	2,194
Water		109
HRWRA	Rheocrete CNI	30.8
Accelerator	Glenium 3030NS	30.0
Steel Fibers	Bekaert Corporation	156

The premix (Portland cement, quartz, sand and silica fume) in Table 2.4 was supplied by Ductal. The steel fibers used were straight bars of 12.7 mm (0.5 inch) long and had a 0.2 mm (0.008 inch) diameter with a minimum tensile strength of 2,600 MPa (377 ksi), an average yield strength of 3,160 MPa (458 ksi), average modulus of elasticity of 205 GPa (29,800 ksi), and average ultimate strength of 3,270 MPa (474 ksi). The steel fibers used for the mix in Table 2.5 were the same as those used in the UHPC mix of Li et al. (2009) with the same percentage per volume.

Table 2.5 UHPC mix proportions (Hassan and Jones, 2012)

Constituents	Product/Manufacturer	Proportion by weight (kg/m^3)
Cement	Portland Cement/Class 52.5 N	657
GGBFS	Appleby Group Ltd	418
Silica fume	Elkem Materials	119
Silica sand	WBB Minerals UK	1,051
HRWRA	FOSROC Ltd	40
Water		185
Steel Fibers	Bekaert Corporation	157

Note: GGBFS - Ground Granulated Blast-Furnace Slag

2.1.2 Mixing methodology

It is not only good to have these constituent materials in the UHPC mix but also to have them mixed together properly for the expected results associated with a high strength concrete like UHPC to be achieved. Therefore, mixing is to maintain the uniformity of these constituents in the UHPC mix. However, during the mixing process of UHPC, the internal and external temperature needs to be monitored coupled with using the right mixing equipment. This invariably means that the mixing methodology adopted for UHPC determines if its expected mechanical properties will be met or not.

The mixing methodology used by Su and Peng (2003) was that the constituents (i.e., cement, silica fume, fine aggregates, blast furnace slag, and quartz sand) were poured into the mixer and mixed uniformly. Then, the admixture was added to water and then slowly added to the dry mixture. They were also mixed uniformly for 2-3 minutes. After which, the steel fiber was added to the mix with the mix being continuously stirred for 2-3 minutes. When the mix was viscous, it was poured into molds and vibrated for 30 seconds on vibrating table. The specimens were removed from the mold and kept in a temperature of (20 ± 2 ºC) and relative humidity of above 90% in standard curing chamber for 28 days.

The mixing methodology adopted by Graybeal (2006) was somehow the same as that used by Su and Peng (2003); but Graybeal (2006) used a premix from Ductal and also their mixing method. The premix was weighed and poured in the concrete mixer and mixed thoroughly for 2 minutes. Half of HRWRA was added to water and poured into the premix slowly for another 2 minutes. There was a waiting time of 1 minute before the remaining HRWRA was added to the premix for 30 seconds. There was still another waiting time of 1 minute before the accelerator was added into the mix for another 1 minute. The mixing continued until the UHPC mix changes from a dry powder form to a thick paste. The timing of this step varies. Afterwards, the steel fibers were added slowly for 2 minutes and the mixing continued for another 1 minute until the steel fibers were uniformly distributed in the mix. The UHPC mix was cast into molds by using scoops, and the specimens were vibrated for 10 seconds using a high frequency vibrating table. The specimens were removed from the vibrating table and excess concrete was cut off their top surfaces to make preparation of cured specimens easier. The exposed surfaces were covered with plastic bags to minimize loss of water. The average time used in doing all these was about 20 minutes.

The specimens were de-molded after 24 hours.

For the mixing methodology by Cornelia et al. (2012), they used locally available materials except silica fume. These materials were mixed together before the water and HRWRA were added. The HRWRA was added to water before adding it to the premix. Mixing continues until suitable flowability was achieved. At the end, the steel fibers were added to the premix. The UHPC mix was poured into molds. The exposed surface of the UHPC mix was pulverized with BA2, a solvent-based, film-forming treatment with a high barrier effect against water evaporation along with an acryl, vinyl-mixed polymerized binding agent. The total mixing time was approximately 14 minutes, and all specimens were de-molded after 24 hours.

2.1.3 Curing methodology

Apart from giving required attention to the mixing process involved in UHPC production, the curing methods adopted for this type of concrete cannot be compromised as this goes a long way in determining its applicability. Also, the physical, mechanical, and durability characteristics of UHPC can be greatly influenced by curing regimens used. Therefore, curing is a way or method of ensuring that the hydration process of the cement is completed effectively by controlling the temperature and ensuring that the relative humidity in the concrete mix is maintained throughout the hydration process. All specimens to be cured are de-molded after 24 hours of casting, setting and placing. Commonly employed curing regimes to achieve desirable mechanical properties for UHPC are: Standard Thermal Treatment, Delayed Thermal Treatment, Tempered Temperature Thermal Treatment, and Air Temperature cure (Graybeal, 2006).

Standard thermal treatment or steam curing is when the specimens are cured at 194ºF

and a 95% relative humidity for 48 hours after demolding. These specimens are cured at a constant temperature of 194ºF for 44 hours and the temperature is either decreased or increased for 2 hours, respectively, to make a total of 48 hours of curing.

Delayed thermal treatment is when the specimens are subjected to the same temperature and relative humidity as that of the standard thermal treatment but the curing procedure is delayed for about 15 days before the curing commences. It invariably means that specimens cured in delayed thermal treatment first undergo laboratory air temperature treatment prior to the delayed thermal treatment.

Tempered temperature thermal treatment is that the specimens are cured at a temperature of about 140ºF and 60% relative humidity after demolding.

Air temperature treatment is that the specimens are left to be cured after demolding with the laboratory air or at the laboratory room temperature without any assisted form of treatment.

Of all the curing methods mentioned above, it has been observed by the researchers that the steam curing assists the UHPC specimen to gain early strength because the hydration process is accelerated by the presence of the steam. Steam-cured UHPC usually exhibited the highest compressive and flexural strength, followed by hot water curing and wet/air curing (Lawend et al., 2013; Wu et al., 2017). However, applications of steaming curing and hot water curing are not practical due to difficulty of implementation. Wet/air curing is more economical and acceptable for field construction.

2.2 Mechanical Properties and Testing Methods for UHPC

Non-destructive testing methods conducted on traditional concrete can also be extended to UHPC to determine its material properties. Ultrasonic pulse velocity testing

method was carried out to determine UHPC modulus of elasticity and Poisson's ratio due to its relatively homogenous nature. It was also used to detect inhomogeneity within the mix. In order to validate the testing method, its dynamic modulus of elasticity was compared with its static modulus of elasticity. The dynamic modulus of elasticity which was about 52 GPa was marginally greater than the static modulus of elasticity (50 GPa). This was attributed to the fact that the specimens subjected for the dynamic modulus of elasticity measurements were under stressed. Also in its calculation, the initial tangent modulus was used as opposed to the use of secant modulus for traditional concrete. The Poisson's ratio of the dynamic and static tests of UHPC were observed to be between 0.18 and 0.24 (Graybeal, 2006; Glaubitt et al., 2008; Hassan and Jones, 2012).

2.2.1 Compressive strength

Collepardi et al. (1997) mentioned that since UHPC or RPC (Reactive Powder Concrete) does not include coarse aggregate, it is essentially not a concrete, even though it is referred to as such. The effect of including well graded coarse aggregate (maximum size of 8 mm) replacing partly or entirely fine graded sand and cementitious material in UHPC was observed in their study, under various curing conditions. The compressive strength was measured using 40 mm cube specimens. At 28 days, the observed strength for specimens cured at room temperature or steam cured at 90ºC was 160 - 180 MPa while it was in the range of 190 - 210 MPa for autoclaved specimens at 160ºC. Since the inclusion of coarse aggregate reduced the amount of cementitious material for the same amount of water, the w/cm ratio was increased; therefore, the strength decreased by a smaller amount, but not significantly.

Considering the compressive strength of UHPC with no coarse aggregate and 2% steel

fiber by volume, Graybeal (2007) conducted experiments on 3-inch diameter, 6-inch high cylinders by applying steam curing and laboratory curing after demolding. Steam-cured specimens exhibited the compressive strength of 193 MPs (28 ksi) while untreated specimens produced a compressive strength of 126 MPa (18.3 ksi) at 28 days.

Kusumawardaningsinh et al. (2015a) compared the compressive strengths obtained from 100 mm diameter, 200 mm high cylinders and 100 mm cubes with fiber contents 0%, 1% to 2% by volume. Although the targeted compressive strength at 28 days was 200 MPa, the 0% fiber UHPC cubes produced a compressive strength of 166.4 MPa, and the cylinders a strength of 186.8 MPa. The 1% fiber UHPC cubes exhibited the compressive strength of 176.27 MPa, while the cylinders reached a strength of 178.28 MPa. The 2% fiber UHPC cubes produced a strength of 178.03 MPa, while the cylinder a compressive strength of 178.35 MPa. It was also concluded that the steel fibers enhanced the compressive strength of the UHPC. This phenomenon was observed in the failure modes as well, when the unreinforced (0% fiber) UHPC specimens failed with sudden, explosive brittle failure, while the fiber-reinforced UHPC specimens exhibited ductile failure.

Karmout (2009) investigated the strength development of UHPC in the Gaza strip. The compressive strength had been measured on 100 mm cube specimens, cast in two layers, each tamped 25 times instead of using an external vibration, and then covered with plastic sheets in the initial 24 hours to prevent loss of moisture. The cubes yielded the compressive strengths of 96, 112, and 128 MPa at 7, 14 and 28 days, respectively.

2.2.1.1 Effect of Different Specimen Sizes

There are different types of compression test specimens for concrete: cylinders and cubes. In the United States, the popular specimen geometry is in form of a cylinder. Even

though this method is efficient and economical when used for testing conventional concrete, a few practical problems are encountered when using the cylinder specimens for testing UHPC's compressive strength. To get accurate results from this test, the ends of the cylinder must have flat, planar surfaces to take the force exerted by the testing machine. ASTM C617 (2015) "Standard Practice for Capping Cylindrical Concrete Specimens" and ASTM C1231 (2015) "Standard Practice for Use of Unbonded Caps in Determination of Compressive Strength of Hardened Cylindrical Concrete Specimens" provide guidelines to prepare the cylinder ends with capping compounds, but the strength of these compounds are limited so that this technique is not useful with UHPC. An alternative technique is to grind the ends of the cylinders, which is however, time consuming and expensive. Using a cube geometry is an alternative to the cylinder which eliminates some of these issues. ASTM C109 (2016) "Standard Test Method for Compressive Strength of Hydraulic Cement Mortars", which is based on 2 inch cubes for testing hydraulic cement mortars, can be used with UHPC, which is essentially a mortar as it does not contain coarse aggregate. Also, the aspect ratio of a specimen subjected to uniaxial loading affects the compression behavior, leading to cubes having greater compressive strengths than cylinders (Neville, 1996).

Graybeal (2015) conducted extensive studies in this area and proposed several relationships between various geometries of cubes and cylinders presented in Tables 2.6 and 2.7. Kusumawardaningsinh et al. (2015a) also proposed the conversion factors for compressive strengths of 100 mm cubes and 100 mm diameter and 200 mm high cylinders: 0.89 (for 0% fiber UHPC), 0.94 (for 1% fiber UHPC) and 0.94 (for 2% fiber UHPC).

Table 2.6 Conversion factors for compressive strength: 4 inch diameter cylinders (Graybeal, 2015)

Tested	Multiply by	Result
3 inch diameter cylinder	0.99	4 inch diameter cylinder
100 mm cube	1.00	4 inch diameter cylinder
70.7 mm cube	0.93	4 inch diameter cylinder
2 inch cube	0.96	4 inch diameter cylinder

Table 2.7 Conversion factors for compressive strength: 3 inch diameter cylinders (Graybeal, 2015)

Tested	Multiply by	Result
4 inch diameter cylinder	1.01	3 inch diameter cylinder
100 mm cube	1.00	3 inch diameter cylinder
70.7 mm cube	0.94	3 inch diameter cylinder
2 inch cube	0.96	3 inch diameter cylinder

2.2.1.2 Test Methods

Since the compressive strength of UHPC can exceed the compressive strength of concrete by a factor of 7 (Graybeal, 2015), using the standard ASTM C39 (2016) “Standard Test Method for Compressive Strength of Cylindrical Concrete Specimens” to measure the compressive strength of UHPC can bring about a few concerns. In addition to the fact that the end preparation of cylinders is problematic (mentioned previously), the loading rate would also be an issue. Using the specified loading rate in the ASTM C39 (35 psi/s) for testing UHPC specimens would result in a longer test duration. Graybeal (2015) studied the effects of using higher loading rates ranging up to 220 psi/s for testing UHPC compression test specimens. Several variables were included in the study: age of concrete

at testing, curing conditions, geometry of specimen, and mix constituents. The typical time duration of testing a conventional concrete specimen at 35 psi/s was 3 minutes. When testing UHPC specimens at a rate of 150 psi/s, the time duration was also approximately 3 minutes. Therefore, this rate was selected as the appropriate reference point to compare results. It was concluded that increasing the load rate had a minimal effect on the observed strength.

2.2.2 Modulus of elasticity

Collepardi et al. (1997) determined the modulus of elasticity of RPC cylinder specimens with 60 or 120 mm diameter with height/diameter ratio of 2. The cylinders were stressed at 13.3 or 53 MPa, respectively. Coarse aggregate was included in the mix by replacing partially or wholly fine sand and some of cementitious materials. All specimens were steam cured and subjected to compressive loading when the strength ranged from 150 -160 MPa. The calculated value of elastic modulus was about 40 GPa (5,800 ksi).

In Graybeal (2007)’s study, the steam treated UHPC had a modulus of elasticity of 52.7 GPa (7,650 ksi) with a 1.5 standard deviation at 28 days. At the same test time, the untreated specimens displayed an elastic modulus of 42.7 GPa (6,200 ksi). It was concluded that the modulus of elasticity of UHPC was predictable within a compressive strength range of 25 - 193 MPa (3.6 - 28 ksi). In a newer study by the same author, the modulus of elasticity values were in the range of 50 - 55 GPa (7,300 - 8,000 ksi). These tests were conducted according to the guidelines given in ASTM C469 (2014) “Standard Test Method for Static Modulus of Elasticity and Poisson's Ratio of Concrete in Compression”. Steam cured as well as laboratory cured cylinder specimens with 3 and 4 inch diameters were tested with axial strain measurement devices to record the change in

length. The same issue as mentioned previously in the compressive strength was also considered in this study. The loading rate was changed to increase up to 200 psi/s. However, the increase in the loading rate from 35 - 150 psi/s did not have a significant effect on the observed elastic modulus of UHPC.

2.2.3 Tensile strength

2.2.3.1 Flexural strength (Modulus of rupture)

Collepardi et al. (1997) investigated the flexural strength of RPC specimens. Flexural strengths were determined at 3, 7, and 28 days, using a third-point loading method on 150 mm x 150 mm x 600 mm (6 inch x 6 inch x 24 inch) beams and a central point loading method on 40 mm x 40mm x 160 mm (1.6 inch x 1.6 inch x 6.5 inch) specimens. Specimens were cured at three different temperatures: 20°C, 90°C, and 160°C, respectively. At 28 days, the flexural strengths in the third-point loading tests were 16.1 - 21.6 MPa, while the central point loading test yielded results 35.5 - 60.1 MPa, indicating that the smaller beams exhibited greater flexural strength. The authors have reported that the flexural strength was reduced when all the fine sand was replaced by the coarse aggregate. The authors explained the reason for the lower flexural strengths in terms of homogeneity and bond strength.

The modulus of rupture values from Russel and Graybeal (2013) were obtained using the standard ASTM C1018 (1997, withdrawn 2006) “Standard Test Method for Flexural Toughness and First Crack Strength of Fiber-Reinforced Concrete (Using Beam with third point loading)’. The strengths for the first cracking varied from 9.0 - 10.3 MPa (1.3 - 1.5 ksi), depending on the method of steam curing, while the values were lower for untreated specimens of about 9.0 MPa (1.3 ksi).

The ASTM C78 (2015) “Standard Test Method for Flexural Strength of Concrete

(Using Simple Beam with Third-Point Loading)" was used by Allena and Newtson (2011) to measure the modulus of rupture. The specimen size was 75mm x 100mm x 400 mm (3 inch x 4 inch x 16 inch), and the specimens were rotated 90º from the orientation in which they were cast to apply the loading. At the age of 7 days, the modulus of rupture were 10 - 18.3 MPa (1.45 - 2.65 ksi) with the highest results for specimens cured at 200ºC which accelarated the pozzolanic reaction of the silica fume.

2.2.3.2 Splitting tensile strength

Karmout (2009) measured the splitting tensile strength according to ASTM C496 (2011) "Standard Test Method for Splitting Tensile Strength of Cylindrical Concrete Specimens", which is an indirect method of measuring the tensile strength of concrete. It is usually used to evaluate the shear resistance provided by the constituents in the concrete matrix. The compressive load applied along the length of the cylinder induces tensile and shear stresses on the aggregate elements in the specimen, generating bond failure between aggregate particles and the cement paste. Karmout (2009) used the cylinder specimens of 150 mm in diameter and 300 mm in height and obtained the tensile strengths of 6.3, 7.1 and 8.1 MPa at 7, 14 and 28 days, respectively.

Graybeal and Hartmann (2003) also used the same testing procedure based on ASTM C496 with a few modifications; the load rate was increased from 100-200 psi/min to 500 psi/min to reduce the testing time duration. Preliminary testing had been done to ensure that this change would not significantly affect the results. Also, lateral expansion of the specimen was measured during the test by a spring-loaded apparatus which held two displacement transducers at each end of the specimen. The specimen size was 4 inch diameter with a 8 inch height. The tensile cracking strength, which was obtained at the

point where the specimen lateral stiffness changes initially, was the greatest for steam cured (194ºF, 95% RH for 48 hours after demolding) specimens; 11.7 MPa (1.7 ksi) at 28 days. Tempered steam cured (140ºF, 95% RH for 48 hours after demolding) specimens showed a slightly lower strength of 11.0 MPa (1.6 ksi); while the ambient air cured specimens indicated a strength of 9.0 MPa (1.3 ksi) at 28 days. The peak strength values were also presented; however, these results were not taken as very accurate representations of the actual tensile strength of UHPC, since the loading configuration of the test causes a biaxial state of stress which produced the significantly increased fiber pullout strength. The steam cured specimens exhibited the highest tensile strength of 24.2 MPa (3.51 ksi) at 28 days; while the ambient air treated specimens had a strengh of 19.0 MPa (2.75 ksi) at 28 days.

2.2.3.3 Direct tension strength

The tensile strength of concrete can also be measured directly. Graybeal and Hartmann (2003) measured the tensile strength in this direct method which is similar to the compression test, except that the ends of the cylinder are adhesively bonded to the testing machine. It is based on the RILEM uni-axial Tension Test for Steel Fibre Reinforced Concrete (RILEM, 2001) and USBR 4914 (USBR, 1992) test methods. The size of the specimen was 4 inch in diameter and 8 inch in height. The age of testing of concrete in this study varied up to 50 days after casting. The cracking strength for the various curing conditions were as follows: Steam cured (194ºF, 95% RH for 48 hours after demolding) specimens had a tensile strength of 11.0 MPa (1.6 ksi) and delayed steam (similar to steam curing but the treatment is applied 15 days after casting) cured specimens had a strength of 11.2 MPa (1.62 ksi). But the air cured specimens had significantly lower strength at 5.65 MPa (0.82 ksi).

Another approach taken by Kusumawardaningsih et al. (2015b) was to cast a series of prisms with a cross section of 40 mm x 40 mm with a notch of 5 mm x 5 mm size and apply tension using a tension testing machine. The test was displacement-controlled with the displacement rate of 0.01 mm/s until the crack opening exceeded 2 mm. Then, the displacement rate was increased to 0.05 mm/s. The test setup and instrumentation are shown in Figure 2.1.

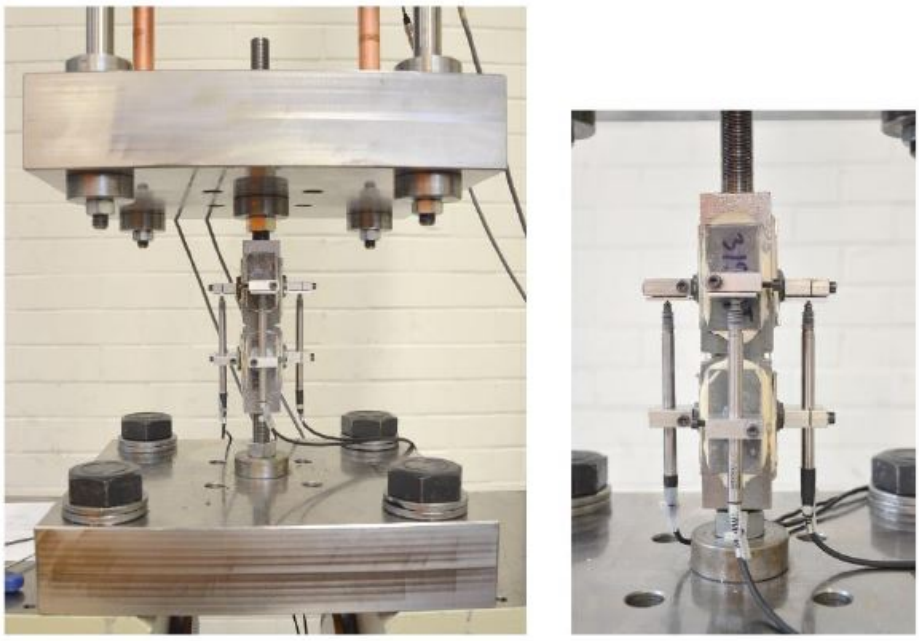

Figure 2.1 The test setup (left) and the instrumentation (right) (Kusumawardaningsih et al., 2015b)

It was observed that in UHPC (with no fiber reinforcement), the maximum tensile strength was approximately 4 MPa with sudden brittle failure. In UHPC (with 2% fiber reinforcement, or called the ultra-high performance fiber reinforced concrete or UHPFRC), the maximum tensile strength was about 6.6 MPa and exhibited an excellent ductile behavior as can be seen in Figure 2.2.

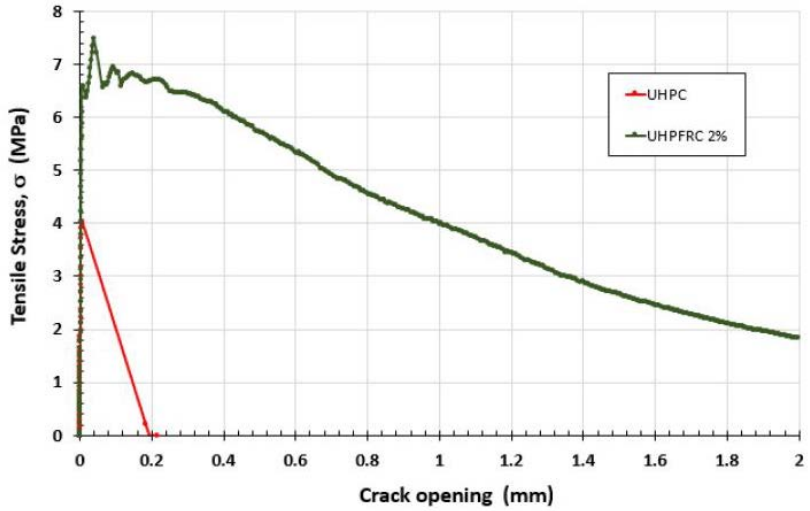

Figure 2.2 Tensile stress- crack opening diagram (Kusumawardaningsih et al., 2015b)

Graybeal and Baby (2013) designed another direction tension test (DTT) specimen in order to capture the tensile behavior of UHPC accurately with a 2 inch square cross section and 17 inch or 12 inch in length. This method was also displacement-controlled with a constant rate of 0.0001 in/s. Tapered aluminum plates were glued with high strength epoxy to the ends of the UHPFRC prism to limit the crack location inside the gauge length and the strain was measured with a parallel ring extensometer (Figure 2.3). The specimens were subjected to both the steam curing and laboratory environment curing. The highest tensile (first cracking) strength was obtained for steam cured, 17 inch long specimens at 9.09 MPa (1.32 ksi). For the laboratory environment-cured specimens, the tensile strength was in the range of 6.67 MPa (0.97 ksi) for the 17 inch long specimens; while the 12 inch long specimens had lower strengths comparatively. The use of longer specimens was hence recommended by the authors.

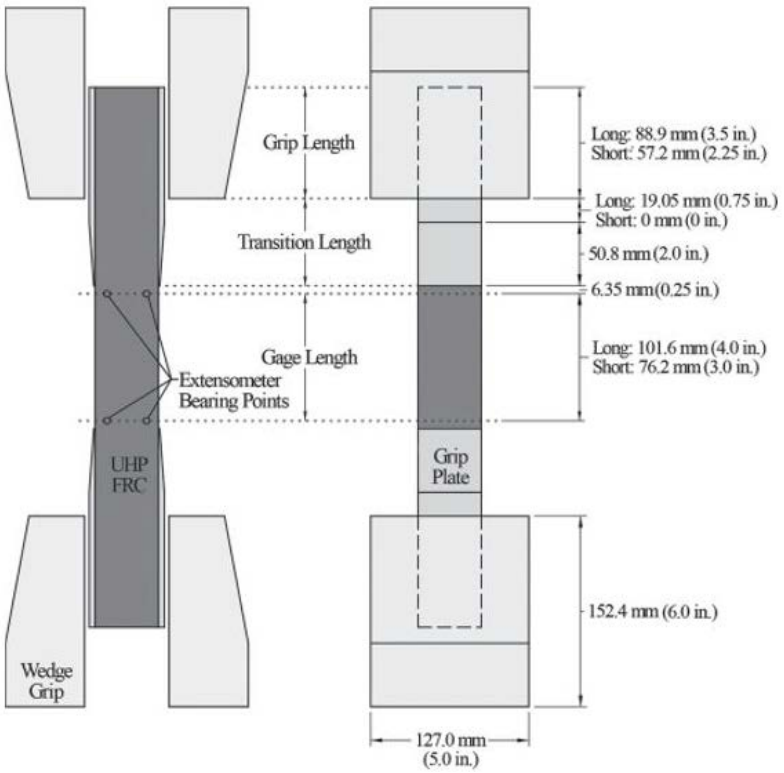

Figure 2.3 Sketch of direct tension test (DTT) specimen (Graybeal and Baby, 2013)

Nguyen et al. (2014) investigated the effects of size and geometry on the direct tensile stress of UHPC using the dogbone shape specimens (Figure 2.4), the gauge length, section area, volume and thickness were considered, and the strength, strain capacity and energy absorption capacity were obtained eventually. The increasing of gauge length, section area and volume of specimens resulted in a little reduction of tensile strength while significant decrease in the strain capacity and energy absorption capacity and clear increase in the crack spacing of specimens. However, it was observed that the tensile strength slightly increased and both the strain capacity and energy absorption capacity distinctly increased when increasing the thickness of the specimen. Tran et al. (2015) also concluded that the specimen size clearly influences the tensile strength of UHPC at the high strain rates.

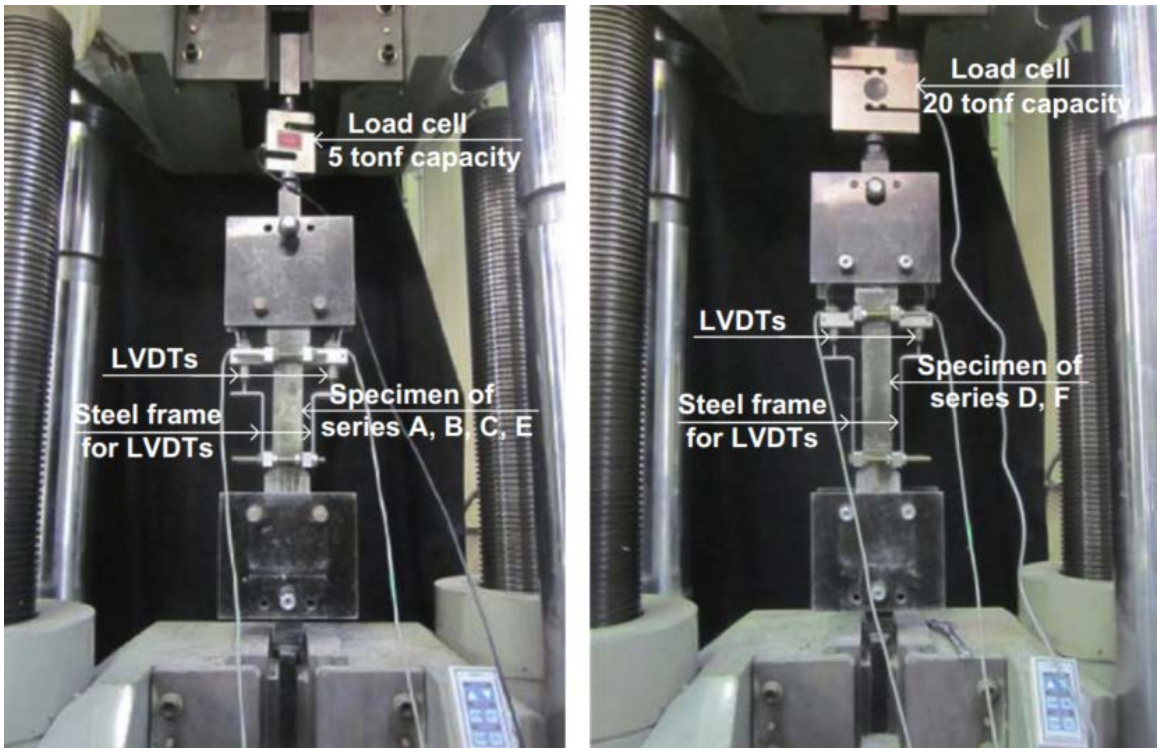

Figure 2.4 Direct tension test (DTT) (Nguyen et al., 2014)

The strain rate dependent properties of UHPC under direct tension were investigated by Pyo et al. (2015). The dogbone shaped specimens with different fiber content and fiber type were tested under different strain rate, which varied from 0.0001 1/s to 0.1 1/s. They observed that the tensile strength and fracture energy increased with the increasing of strain rate and fiber volume.

2.2.4 Bond strength

The application of UHPC for use in connection details in structures is becoming increasingly popular and thus requires extensive research into the bond strength properties between UHPC and reinforcing bars.

Yuan and Graybeal (2014) designed a new test specimen to simulate the lap-splice configuration in a connection system (Figure 2.5). The pullout specimen was a strip of UHPC with embedded rebars (testing bars), cast on top of a concrete slab with more rebar

joining the two concrete sections. The embedment length, the clear side cover, the clear spacing between the testing bar and the joining rebar, the type and size of rebar, the casting orientation and the concrete compressive strength were the parameters tested in their study.

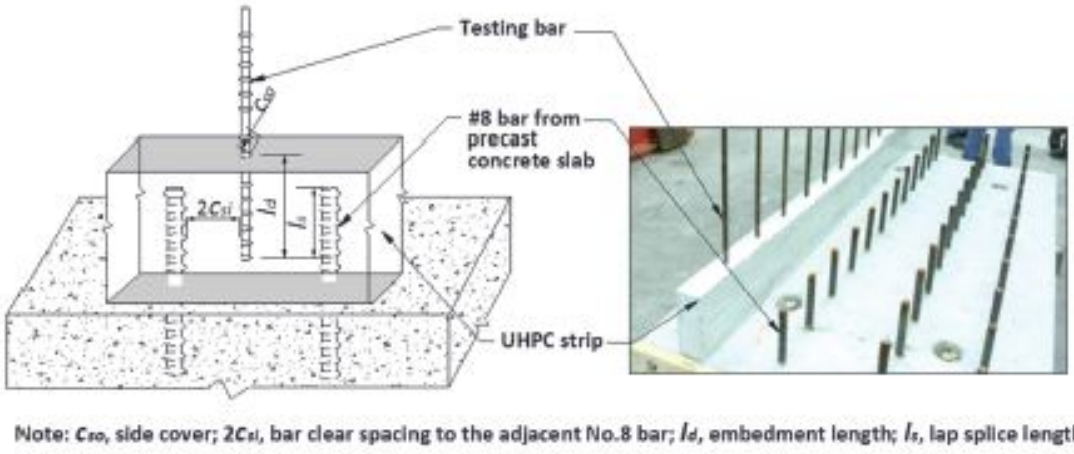

Figure 2.5 Configuration of pull-out test specimens (Graybeal and Baby, 2013)

Each parameter was tested in several groups where all other variables were kept constant. It was observed that increasing the embedment length increased the bond strength. As in normal concrete, the bar stress was nearly linear with the bond length. The cover and the bar spacing were also studied, and the effect on the failure mode was observed. Depending on whether the cover is smaller than the clear spacing between the bars, the failure would occur as a splitting crack across the outer cover or between the adjoining bars. Also, the bond strength decreased when the bar spacing was very small as the contact splice because it limited the ability of the fiber reinforcement to enhance the strength of the UHPC. Regarding the compressive strength, it was observed that when the compressive strength is increased, the bond strength increased. The bond strength was calculated by the following formula:

$$\mu_{Test} = \frac{f_{s,max}\pi d_b^2}{\pi d_b l_b} \tag{2.1}$$

where, μ_{Test} – bond stress;

$f_{s,max}$ – maximum bar stress;

d_b – bar diameter;

l_d – bond length.

When the bar diameter increased, the bond strength decreased. Also, the epoxy coated bars had lower bond strength than the uncoated bars. The authors recommended that, in order to obtain the bar yield stress at bond failure, the bar size should be from No. 4 to No. 8 and the minimum compressive strength be 93.08 MPa (13.50 ksi). Also a minimum embedment length of $8d_b$ and a minimum side cover of $3d_b$ with a clear bar spacing between $2d_b$ and l_s (the lap splice length) were recommended for design of the connection system.

2.2.5 Shrinkage and creep of UHPC

The quantity of water in a concrete mix greatly affects its shrinkage characteristics. Shrinkage is a result of the changes in the volume of the concrete due to loss of water from the mix. Concrete with high w/cm tends to shrink more than those with low w/cm because the excess water flows to the concrete surface. When this occurs, the excess water evaporates from the surface of the concrete and leaves cracks on the concrete surface. The types of shrinkage associated with concrete are plastic, autogenous, drying and carbonation shrinkage (Shetty, 2005).

Plastic shrinkage occurs when the concrete is in its plastic state and there is excess water in the concrete mix or when the aggregate rapidly absorbs the water in the mix. The excess water bleeds to the surface of the concrete during evaporation or drying, and the concrete surface collapses due to loss of water in the mix, leading to crack.

Autogenous shrinkage is the type of shrinkage that occurs when there is no temperature interaction between the concrete mix and its surroundings.

Drying shrinkage occurs as a result of loss of water from the gel of the concrete due to placing the concrete in dry conditions or surroundings.

Carbonation shrinkage occurs as a result of the atmospheric carbon-dioxide reacting in the presence of water with the hydrated cement.

It was observed that the steam-cured UHPC does not shrink but swell when exposed to drying conditions. This must be due to the enhanced hydration process by the steam curing treatment and the exhaustion of the mix water during this process. Also, UHPC was not influenced by plastic shrinkage because of the high cementitious and low w/cm present in its mix (Ioan and Cornelia, 2010).

Ioan and Cornelia (2010) investigated the effect of two methods of shrinkage on UHPC with steel fibers and without steel fibers. Both specimens underwent two methods of shrinkage for early shrinkage: the autogenous shrinkage and total shrinkage. While only total shrinkage method was considered for long term shrinkage. Specimens that went through autogenous shrinkage were covered with aluminum foil to prevent loss or gain of moisture to and from the environment. They had embedded steel rods with which strain gauges were attached at its free ends. The shrinkage measurement was taken 30 minutes for the first 12 hours and twice a day for over 7 days. The specimens that went through the total shrinkage were not covered with aluminum foil. Shrinkage measurement was also taken in similar manner as the autogenous shrinkage specimens. Specimens for the autogenous and total shrinkage were kept in the temperature of 20 ºC and relative humidity (RH) of 60%.

The specimens that were air cured had lesser drying shrinkage as they only experienced swelling and after demolding in comparison with those that were restrained from moisture that experienced large amount of deformation.

Specimens for the long term shrinkage were initially steam cured for 5 days at 90ºC and 80% RH. At the 6th day, they were cured with the room temperature at 20ºC and 60% RH. The measurement was taken daily for a month and weekly for the rest 120 days. It was observed that the specimens with and without the steel fibers neither swelled nor shrank. However, the UHPC with fibers swelled lesser than those without fibers. All specimens were de-molded after 24 hours of casting. It can be observed from their results that UHPC was unaffected by drying shrinkage but greatly affected by autogenous shrinkage.

The shrinkage-swelling behavior was observed by Collepardi et al., (1997) in mixtures with coarse aggregate partially or wholly replacing sand or cementitious material, after a curing time of 7 days. The specimens were exposed to a 65% RH air for 30 days and submerged in water. There was no significant difference in shrikange or sweeling between the mixes including coarse aggregate and not. Shrinkage was also lower in steam cured and autoclaved specimens when compared to the air cured specimens. After a month of exposure to 65% air, the shrinkage was about 600 με.

Graybeal and Hartmann (2003) did a limited shrinkage study to observe the early age shrinkage behavior of UHPC. The specimen was of 25 mm x 25mm x 275 mm (1 inch x 1 inch x 11 inch) in size and 6 bars each were tested for each curing condition. The standard procedure was based on ASTM C157 (2014) “Standard Test Method for Length Change of Hardened Hydraulic-Cement Mortar and Concrete”, and the intial readings were taken immediately after demolding. The air cured specimens exhibited the most shrinkage of 620

με in 28 days; while the steam cured specimens exhibited the lowest shrinkage of about 500 με in 4.1 days.

Since measuring the autogeneous shrinkage is a somewhat complex task, there is no standard method. Eppers and Muller (2008) measured the linear autogenous shrinkage under quasi-isothermal conditions (20 ºC) using prisms with a dimension of 25 mm x 25 mm x 285 mm). The specimens were sealed with stainless steel foil, tape and beeswax and therefore, the temperature changes and heat of hydration were neglected. Mechanically coupled sensors were employed to measure the shrinkage. The shrinkage at the age of 28 days was approximately 600 - 900 με. The strains were higher with lower water/cement ratios and also with high silica fume contents. Steel fibers reduced the strain by about 10 - 15%.

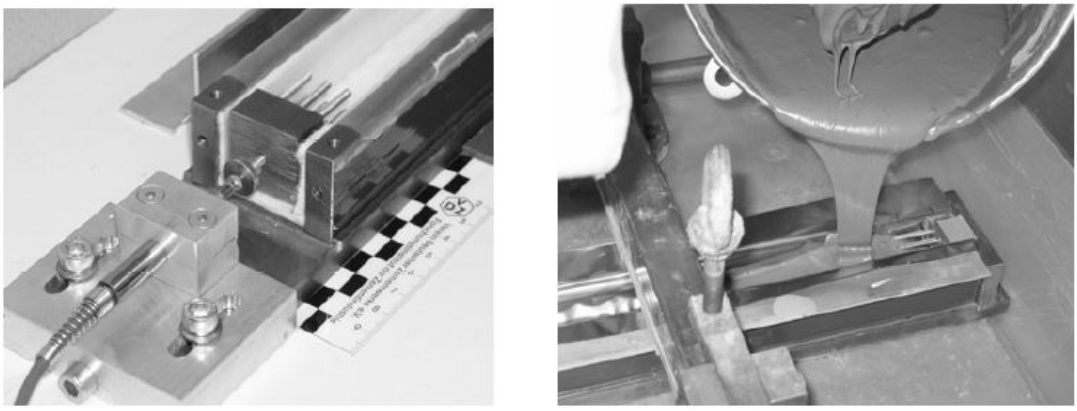

Figure 2.6 Experimental setup for measurement of the autogenous shrinkage and production of a prism (Eppers and Muller, 2008)

Collepardi et al. (1997) presented results from creep tests performed on RPC as well, and they reported that the creep strain of the UHPC specimens under a stress of 53 MPa (7,685 psi) with a stress-strength ratio of 1/3 at the time of loading was greater than that of normal strength concrete with compressive strength ranging from 30 to 40 MPa (4,350 to 5,800 psi). However, the ultimate specific creep including elastic strain was 35 x 10^{-6} MPa^{-}

[1] (0.241×10^{-6} psi^{-1}), regardless of the stress-strength ratio and aggregate to cement ratio of the original or modified RPC. It was also reported that the specific creep of autoclaved specimens was lower than that of specimens cured at room temperature, and the creep of specimens cured at room temperature was the same as that of normal strength concrete.

2.3 Durability of UHPC

2.3.1 Chloride penetration

The presence of chloride ions near the reinforcing steel in concrete structures is a major cause of corrosion. If the chloride ion concentration exceeds the threshold value, the passivating layer on the reinforcing steel is destroyed and chloride ions act as a catalyst for corrosion. Therefore, the study of chloride ion concentration and the impermeable nature of the concrete is of importance.

In an effort to study the effect of different curing conditions on the rapid chloride penetration in UHPC, Ahlborn et al. (2008) followed the procedure specified by ASTM C1202 (2012) "Electric Indication of Concrete's Ability to Resist Chloride Ion Penetration" to prepare specimens and to carry out the test. A 60V electric potential was applied to a saturated cylinder of size 51 mm thick and 102 mm in diameter for 6 hours and the total charge passing was measured. The curing regimes tested were 7 days thermally treated, 28 days air treated, and 28 days thermally treated, and the charge was 11, 75, and 15 coulombs, respectively, which indicated negligible chloride ion permeability (< 100 coulombs). The thermally treated specimens had lower permeability than air treated specimens and was also independent of the testing time.

Graybeal and Hartmann (2003) also investigated the rapid ion chloride penetrability of UHPC according to ASTM C1202. Over the 6-hour time frame, the electrical current

was recorded every 1 minute to compute the total charges passed. The specimens were tested at both 28 and 56 days, with different curing regimes applied up until the time of testing. Regardless of the curing condition, the rapid chloride ion permeability was negligible; however, the penetrability of ambient air cured specimens decreased between 28 and 56 days.

2.3.2 Freeze-thaw durability

Ahlborn et al., (2008) also tested the freeze-thaw durability of UHPC which is important especially for its application in cold climates. ASTM C666 (2015) Procedure B was followed and six 75 mm x 100 mm x 406 mm (3 inch x 4 inch x 16 inch) UHPC specimens were cast and tested in a freeze-thaw chamber, with rapid freezing in air and thawing in water. In addition to these specimens, another 6 specimens (for the different curing regimes) were cycled in and out of a separate bath at ambient temperature to compare mass changes and Relative Dynamic Modulus (RDM). At 28 days, for more than 300 freeze-thaw cycles, RDM were 101.57% and 100.29% for air cured and thermally treated specimens. The RDM values had increased independent of curing regimes.

Graybeal and Hartmann (2003) studied the freeze-thaw resistance of UHPC according to ASTM C666. The temperature of the freeze-thaw cycles were 0ºF and 40ºF. At every 30 cycles, the dynamic modulus of elasticity of the specimens were measured. The basis of the test is that the repeated cycles will cause microscopic degradation of the UHPC resulting in decreased dynamic modulus of elasticity. The specimen size was 3 inch x 4 inch x 16 inch, and they were cured for 28 days prior to initiating the freeze-thaw cyclic test. The curing conditions tested were Steam, Tempered Steam, Delayed Steam and Ambient Air. While all steam-cured specimens had the dynamic modulus close to the

original value, the ambient air cured specimens displayed an increase in the dynamic modulus.

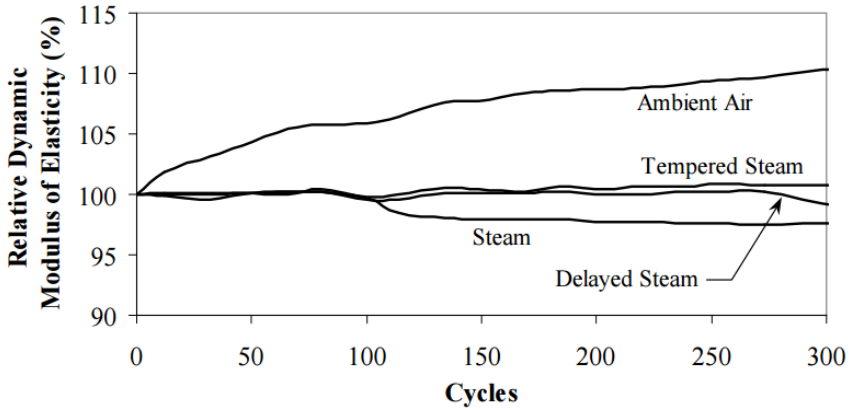

Figure 2.7 Freeze-thaw resistance of UHPC (Graybeal and Hartmann, 2003)

2.4 Applications of UHPC as Connectors for Precast Bridge Girders

It has been a major concern for bridge owners on how to connect precast bridge girders on site as the overall performance of bridges also depend on connectors as well as the members to be connected. Various connectors have been proposed but failed in terms of fatigue, durability and long term performance. In order to achieve these desired performance, UHPC was proposed to be used as a connector between the precast bridge girders. UHPC offers it advantages of smaller and thinner sections to reduce the volume of concrete needed as connectors between these precast members. Not only does UHPC reduce the volume of concrete needed for connection (e.g., narrow connection joints), but also reduces the development length of the connecting girders (Graybeal, 2010). To utilize these imminent advantages of UHPC, the precast girders were pre-wet prior to their connection with the wet UHPC mix to ensure good bonding between the two components (Graybeal, 2012).

In order to validate the use of UHPC as a connecting member between bridge girders,

Graybeal (2010) carried out an experimental program on the fatigue performance and ultimate capacity by using six specimens consisting of two traditional concrete mixes produced at the Fort Miller Company, Inc. in Schuylerville, New York. Among these six specimens, four were in transverse connections between full-depth deck panels and the remaining two were in longitudinal connections between the top flanges of deck-bulb-tee girders. The girders with the compressive strength of 6.5 ksi at 28 days were cast first with their joint reinforcement extending through the shear key faces. The UHPC mix supplied by Ductal according to the composition of Table 2.1 was mixed and poured into the connecting joints between the two traditional concrete. The surface of the UHPC mix was covered with water proof membrane and asphalt to prevent evaporation of the mix water. Both the traditional concrete and the UHPC mix were cured in air temperature. The 28 days compressive strength for the UHPC was 24.2 ksi. Each specimen was cyclically loaded to simulate the fatigue performance of the joint under repeated truck wheel loading. The number of cycles and applied load were increased until the specimen showed the sign of crack. The specimens were assessed for interface de-bonding due to leakage, concrete cracks and strain distribution. Afterwards, the monotonic loads were applied to the specimen to failure so that the ultimate load-carrying capacity was measured. Tensile flexural cracks were observed in the girders when the cyclic load was increased from 16 kips to 21.3 kips. However, the UHPC did not show any visible cracks during the testing and there was no leakage from the UHPC mix as well.

The cast in-situ UHPC has been successfully used to connect the top flanges of about 18 bridge girders in the US among which are Route 31 bridge in Lyons, NY, Route 23 bridge in Oneonta, NY, and Keg Creek Bridge in Council Bluffs, IA. It has also been used

as PI-girders for the replacement bridge project which is located on a county road (136th Street) over the east branch of Buffalo Creek in northeast, Buchanan County, Iowa (Graybeal, 2010; Brain et al., 2007).

2.5 Other applications of UHPC

The UHPC has been used in other applications: The Sherbrooke Bridge in Quebec, Canada, built in 1997, a pedestrian bridge of 190 ft. with a deck thickness of only 1.25 inch. Similarly, the footbridge of Peace in Seoul, Korea, was built in 2002. The span of this bridge is 400 ft. and its deck thickness is 1.25 inch. The roof thin-shelled canopies of Shawnessy Light Rail Transit (LRT) Station, Calgary, Alberta, Canada was constructed with UHPC. UHPC was mostly used for highway bridge girders because of the reduced maintenance cost in comparison with steel girders or traditional concrete girders (Victor et al., 2009; Perry and Zakariasen, 2004).

Portugal employed UHPC for seawall anchors, Australia considered its use in a vehicular bridge, and France applied it in building power plants. On the U.S. Route 6 Bridge over Keg Creek in Pottawatomie County, IA, UHPC was used in the longitudinal and transverse joints between the concrete deck panels. In all of these cases, the material was chosen for its ability to withstand high stress, both environment- and load-related.

With the use of steel fiber content of 6% by volume, 12 mm length and diameter of 0.4 mm, UHPC was applied on site to connect precast slabs of two buildings at Aalborg University, Denmark, forming a continuous slab with no beams. The connection also made possible short anchorage length of reinforcement to be used (Hansen and Jensen, 1999).

2.6 Advantages of UHPC

Lighter and thinner sections are possible with UHPC and can be used for structural members thereby reducing the demand on supporting members. Also, UHPC has high durability than the conventional concrete or high performance concrete (Aziz and Ahmed, 2012).

In summary, the UHPC and its applications can lead to the following advantages over the conventional concrete materials and structures:

- Superior mechanical strength and ductility;
- Reduced or smaller sections and significant weight reductions;
- Reduced number of structural elements;
- Greater energy absorption during seismic and impact events;
- Dense microstructure and discontinuous pore structures which provide excellent protection against corrosion, excellent chloride penetration resistance and low water absorption, and excellent freeze-thaw durability.

Chapter 3 MATERIALS

The primary goals of this study are to develop the UHPC mixtures with locally available materials and to investigate the mechanical properties, shrinkage, ductility, and bond properties. In the following sections, the materials used in this study are presented.

3.1 Constituents

The Portland cement Type I-II with a specific gravity of 3.15 was used to prepare the UHPC samples in this study. Commercially available silica fume (Rheomac SF 100) provided by BASF Construction Chemicals, LLC was used as a partial replacement of cement to improve the mechanical properties and durability of UHPC.

Local natural sand was provided by the Atlas Sand & Rock, which is located in Pullman, WA. The sand passed through the ASTM No. 30 (0.6 mm) sieve and over the No. 200 (0.075 mm) sieve was washed to remove the clay/silt particles and then oven-dried at 110°C (230°F) to achieve zero moisture content. Table 3.1 presents the grain size distribution of the fine sand from sieve analysis according to ASTM C136 (2014). The specific gravity and water absorption of the fine sand were determined according to ASTM C128 (2015), and they are 2.60 and 2.6%, respectively.

Table 3.1 Grain size distribution of fine sand

	Fine Aggregate	
Sieves	Individual % Retained	Cumulative % Passing
#30	0	100
#50	71	29
#100	22.7	6.3
#200	6.3	0

Domestically available steel fiber (NYCON-SF Type I, Figure 3.1) provided by Nycon Corporation was used to enhance the durability and toughness of UHPC. Steel fibers were added in the UHPC at a content of 2 percent by volume. The physical properties of steel fiber are presented in Table 3.2, which meets the requirements of ASTM A820 (2015).

Figure 3.1 Steel fiber (NYCON-SF Type I)

Table 3.2 Physical properties of steel fiber

	Steel fiber
Fiber Length, in. (mm)	0.5 (13)
Filament Diameter, in. (mm)	0.008 (0.2)
Specific Gravity	7.8
Aspect Ratio	65
Tensile strength, ksi (MPa)	400 (2,660)
Flexural strength, ksi (GPa)	29,000 (203)
Melting Point, °F (°C)	2760 (1516)
Color	Copper
Water Absorption	Nil
Alkali Resistance	High
Corrosion Resistance	High

Glenium 3030 NS, a commercially available polycarboxylate-based high range water reducing admixture (HRWRA) produced by BASF Construction Chemicals, LLC was used in the UHPC mixes to achieve the desired workability.

3.2 Mix designs

Primarily based on the flowability of the 12 trial mixtures (ASTM C1427, 2015) and varying the water-cementitious materials (w/cm) ratios, different amounts of silica fume, cement and HRWRA, two mixture proportions of UHPC (A4 and C3, see Table 3.3) were chosen. The corresponding water to cementitious materials ratios (w/cm) of mix designs A4 and C3 were 0.21 and 0.18, respectively.

Table 3.3 UHPC mixture proportions

Mixture Type	Unit	A1	A2	A3	**A4**	A5	B1	B2	B3	B4	C1	C2	**C3**
Type I/II Portland Cement	lb/yd^3	1500	1475	1500	**1500**	1500	1450	1390	1278	1500	1620	1560	**1500**
Silica Fume	lb/yd^3	375	150	375	**375**	375	195	190	320	375	260	260	**260**
Fine Sand	lb/yd^3	1396	1823	1297	**1355**	1374	1864	1906	1860	1436	1463	1521	**1574**
Steel Fibers	lb/yd^3	267	197	267	**240**	267	197	197	197	237	236	236	**236**
HRWRA	gal/yd^3	7	7	7	**7**	8	8.7	9.0	9.5	9.0	9.5	10.5	**11.5**
Water	lb/yd^3	375	330	413	**394**	375	288	290	280	347	347	335	**325**
w/cm		0.20	0.20	0.22	**0.21**	0.20	0.18	0.18	0.18	0.18	0.18	0.18	**0.18**
Spread Testing	in.	6.50	7.00	7.75	**9.00**	7.75	5.00	6.00	5.50	5.75	7.25	8.00	**9.50**

3.3 Mixing, casting and curing

Mixing of constituents to produce specimens of UHPC for Category 1 and Category 2 (see details in Chapter 4) was done at the WSU's concrete laboratory by a portable mixer with a volume of 10 gallons (Figure 3.2a) and a concrete drum mixer with a volume of 3.5 cubic feet (Figure 3.2b), respectively. The entire mixing time is relatively longer than that of conventional concrete due to the elimination of coarse aggregate and use of low w/cm ratio, and depends on the power of the mixer (Russel and Graybeal, 2013). In this study, the whole mixing time of the portable laboratory mixer (see Figure 3.2a) ranged 16-20 minutes and consisted of four stages: (1) mix the dry constituents for 2-3 minutes, (2) add 75% of the water and mix 4-5 minutes, (3) add the HRWRA and the remaining 25% of water and mix 2 minutes, and (4) add steel fiber and continue mixing for 8-10 minutes till thorough. The drum mixer took a longer time than the portable mixer, and it took approximately 45 minutes for completing the mixing process.

(a) Portable laboratory mixer for Category 1

(b) Drum mixer for Category 2

Figure 3.2 Mixers of UHPC

As soon as the mixing was completed, the fresh UHPC was poured into oiled wooden/steel molds to cast specimens in accordance with ASTM C192 (2016). Specimens were externally vibrated for approximately 5-10 seconds using a vibrating table. Time of vibration depends on the consistency of mix. After approximate 24 hours, specimens were demolded and began curing period.

Due to very low water content of UHPC, it is extremely critical to prevent loss of internal water due to evaporation and keep specimens in a high moisture environment immediately after casting. The curing of UHPC specimens consists of two phases: initial curing after casting and standard curing prior to testing. All specimens in the molds were cured in a vibration-free fog room with temperature 73.5 ± 3.5 °F (23.0 ± 2.0 °C) from the time of casting. All specimens were then demolded after 24 ± 4 hours from casting and then soaked in lime-saturated water storage tanks until testing age.

Chapter 4 EXPERIMENTAL TESTING PROGRAM

In this chapter, the experimental testing programs to evaluate fresh and hardened properties of UHPC are presented, and these tests include flowability, compressive and tensile strengths, modulus of elasticity, shrinkage, and bond strength.

4.1 Introduction

A number of tests were conducted to evaluate the properties of UHPC in fresh and hardened states. A flow table test was conducted to evaluate the workability of UHPC. The hardened UHPC property tests included two categories. The Category 1 is related to the mechanical properties of UHPC at different ages, such as compressive strength, flexural strength, direct tensile strength, splitting tensile strength, modulus of elasticity, shrinkage, etc. The Category 2 is related to the bond behavior of UHPC, which is of critical concern in field application. The procedures for each test are briefly discussed in the following sections, and the tests considered in this study are summarized in Table 4.1 along with their ASTM/AASHTO standard test method designations. For the tests, three replicates were tested. It should be noted that most of adopted standard tests considered for UHPC in this study are primarily developed for characterization of conventional concrete and cementitious (mortar) materials; while the direct tension test and pullout (bond strength) test used are not the standard test methods.

Table 4.1 Experimental testing program

Properties of Concrete	Test Methods
Fresh Properties of UHPC	
Flow	ASTM C1437
Hardened Properties of UHPC	
Compressive Strength of Concrete	ASTM C109 ASTM C39
Modulus of Rupture (Flexural Strength) of Concrete	ASTM C78
Modulus of Elasticity of Concrete	ASTM C496
Splitting Tensile Strength of Concrete	ASTM C469
Direct Tensile Strength of Concrete	---
Autogenous Shrinkage of Concrete	ASTM C157
Drying Shrinkage	ASTM C157
Restrained Shrinkage Cracking	AASHTO T334
Pullout (Bond Strength) of Concrete	---

4.2 Property Tests of Fresh UHPC

The flow table test for hydraulic cement mortar is widely employed on fresh UHPC to evaluate its rheology. Once the mixing was completed, the flow test was conducted following the procedures of ASTM C1437 (2015, Figure 4.1), i.e., immediately dropping the flow table 25 times in 15 seconds after lifting the flow mold away, and then measuring the average diameter of flow of UHPC mix.

Figure 4.1 Flow test of UHPC

4.3 Property Tests of Hardened UHPC

Several basic mechanical properties were evaluated for the hardened UHPC: compressive strength, modulus of elasticity, flexural strength, splitting tensile strength, and direct tensile strength.

4.3.1 Compressive strength

To investigate the size effects on the compressive strength of UHPC, three types of specimens were tested: 2 inch cubes, 4 inch cubes, and 4 inch x 8 inch cylinders. The compressive strength tests were conducted following the procedures of ASTM C109 “Standard Test Method for Compressive Strength of Hydraulic Cement Mortars (Using 2 in. or [50-mm] Cube Specimens)” (2016) (Figure 4.2a and 4.2b) and ASTM C39 “Standard Test Method for Compressive Strength of Cylindrical Concrete Specimens” (2016) (Figure 4.2c). All the compressive tests were conducted under a specific stress rate, 35 ± 7 psi/s. Therefore, the required loading rate was calculated corresponding to the size of the specimen, i.e., 8400 ± 1680 lbf/min, 33200 ± 6720 lbf/min, and 26400 ± 5300 lbf/min for 2 inch cubes, 4 inch cubes, and 4 inch x 8 inch cylinders, respectively.

(a) 2 inch cube (b) 4 inch cube (c) 4 inch × 8 inch cylinder

Figure 4.2 Compressive strength tests of UHPC

4.3.2 Modulus of elasticity

The modulus of elasticity test was conducted following the procedures of ASTM C469 “Standard Test Method for Static Modulus of Elasticity and Poisson's Ratio of Concrete in Compression” (2014, Figure 4.3). The load was applied corresponding to a specific stress rate, 35 ± 7 psi/s, until it reached 40 % of the average ultimate load of the 6 inch × 12 inch cylinder specimens.

Figure 4.3 Modulus of elasticity test of UHPC (6 inch × 12 inch cylinder)

4.3.3 Tensile strength

4.3.3.1 Flexural strength (Modulus of rupture)

The flexural strength test was performed in accordance with ASTM C78 “Standard Method of Test for Flexural Strength of Concrete (Using Simple Beam with Third-Point Loading)” (2016, Figure 4.4). A constant loading rate was applied under a specific tensile stress rate within the range of 125 to 175 psi/min, i.e., 5,000 to 7,000 lbf/min for the 3 inch x 4 inch x 16 inch prisms.

(a) mold for casting the specimen (b) testing setup

Figure 4.4 Flexural strength test of UHPC (3 inch x 4 inch x 16 inch prism, span: 12 inch)

4.3.3.2 Splitting tensile strength

The splitting tensile strength test was conducted following the procedures of ASTM C496 “Standard Test Method for Splitting Tensile Strength of Cylindrical Concrete Specimens” (2004) (Figure 4.5). The required range of splitting tensile stress is 100 to 200 psi/min; thus, the corresponding loading rate shall be in the range of 11,300 to 22,600 lbf/min for the 6 inch x 12 inch cylinders.

Figure 4.5 Splitting tensile strength test of UHPC (6 inch × 12 inch cylinder)

4.3.3.3 Direct tensile strength

The UHPC dogbone specimens for direct tension were designed and fabricated with the net cross section of 2 inch x 2 inch and gage length of 6 inch (Figure 4.6). Two bolts with caps were embedded inside the ends of the sample for connecting the specimen to the testing machine grasps. An extensometer with 2 inch gage length was used to measure the tensile strain. To assure the tensile strength under quasi-static state, a very low loading rate (i.e., 0.0001 in/s) was chosen in this study.

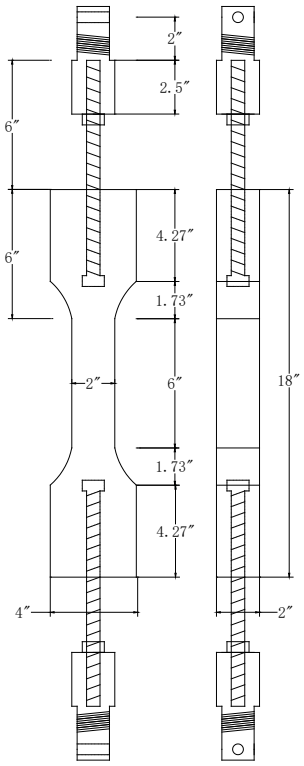

(a) Dimensions of dogbone specimen

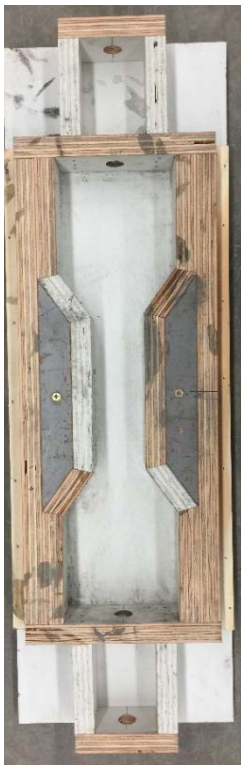

(b) Mold

(c) Specimen

(d) Testing setup

(e) Control panel

Figure 4.6 Illustration of the test setup, specimen shape and measurement system

4.3.4 Shrinkage

Autogenous shrinkage is the shrinkage due to hydration of the binder in UHPC, while drying shrinkage is the shrinkage due to moisture loss when it is exposed to a dry environment. The shrinkage test of UHPC was conducted in accordance with ASTM C157 “Standard Test Method for Length Change of Hardened Hydraulic-Cement Mortar and Concrete”. Two geometries of prism specimens were fabricated to investigate the size effect on shrinkage: (a) 1 inch x 1 inch x 11.25 inch, and (b) 4 inch x 4 inch x 11.25 inch, respectively. The length change of 4 inch x 4 inch x 11.25 inch prism was measured after 24 hours from casting by a linear variable differential transformer (LVDT) glued at two ends and automatically collected by DASYLAB software; while the shrinkage of 1 inch x 1 inch x 11.25 inch prism was measured by the digital gages at two ends (Figure 4.7). UHPC specimens for autogenous shrinkage test were sealed with a thin layer of epoxy on the surface and followed with plastic wrap to prevent moisture loss. The prisms without sealer were used to monitor the free shrinkage, which consists of autogenous shrinkage and dry shrinkage. UHPC specimen for drying shrinkage test were cured at a curing room with temperature of 73±3°F (23±2°C) and relative humidity of 50±4%.

(a) Autogenous Shrinkage Test of 4 inch x 4 inch x 11.25 inch prism

(b) Free Shrinkage Test of 4 inch x 4 inch x 11.25 inch prism

(c) Autogenous Shrinkage Test of 1 inch x 1 inch x 11.25 inch prism

(d) Free Shrinkage Test of 1 inch x 1 inch x 11.25 inch prism

Figure 4.7 Shrinkage tests of UHPC

The free shrinkage tests mainly provide the basic moisture related shrinkage

characteristics of UHPC without any restraint; but in most cases, concrete is under different boundary conditions and shrinkage-induced tension may lead to cracking behaviors. Both the ASTM and AASHTO standards provide test method for restrained shrinkage measurement and suggest that the ring test is used to determine the relative cracking tendency among different concrete mixtures under a certain drying condition. Both the ASTM and AASHTO test methods are based on the same theory and procedures, however, the dimensions of concrete ring and allowable nominal sizes of coarse aggregate show some differences.

In this study, the AASHTO T334-08 (2012) "Standard Method of Test for Estimating the Cracking Tendency of Concrete" is adopted for restrained shrinkage measurement. The inside steel ring is cut from a steel tube for industry (allowable in AASHTO standard), and it has an outer diameter of 12.75 inch, a wall thickness of 1/2 ± 1/64 inch, and a height of 6 inch (Figure 4.8a). The outside ring is made of a plastic board with a thickness of 0.25 inch and an inner diameter of 18 inch, and it is supported around by plywood. The steel strains are measured by four strain gages equidistantly mounted on the inner surface of the inside steel ring and automatically recorded by SmartStrain software at an interval of 1 second (Figure 4.8d). The UHPC ring was casted intermediately after mixing and covered with wet burlap followed with plastic sheet to prevent moisture loss from specimens for the first day. After this initial curing, the outer plastic board was demolded and the top surface was coated with a thin layer of paraffin wax to prevent moisture loss (Figures 4.8b and 4.8c). The ring specimen of UHPC was allowed to present water evaporation through the outside surface only. Similar with free shrinkage, all UHPC specimens used in restrained shrinkage test were cured at a curing room with temperature of 73 ± 3°F (23 ±

2°C) and relative humidity of 50 ± 4%.

(a) Restrained steel ring setup

(b) After casting with UHPC

(c) Demolding after 1 day and coating the top surface with paraffin wax

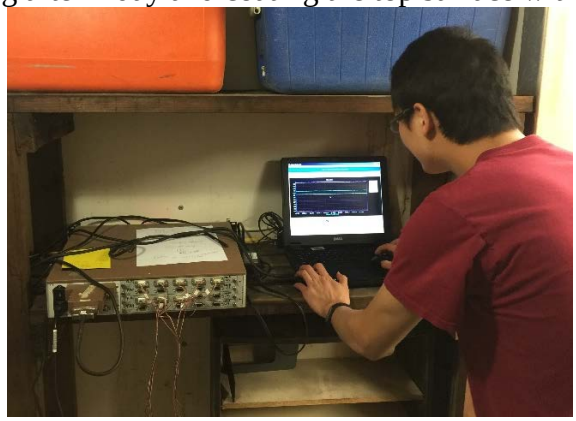

(d) Data acquisition system

Figure 4.8 Restrained shrinkage test of UHPC

4.3.5 Freeze-thaw durability

The UHPC prism samples manufactured were conditioned using the rapid freeze-thaw test in accordance with ASTM C666 Procedure A (2015), which is designed to

evaluate the potential frost resistance of concrete in cold climates. The temperature range of 0^{o} to 40^{o}F is considered in the freeze-thaw cycles, and the cycle frequency is 6 freezing-thawing (F-T) cycles per day. The condition chamber used in the project is shown in Figure 4.9, and three C3 samples were conditioned in the chamber as the “conditioned group”, while another three C3 were soaked in the water as the “control group”.

Figure 4.9 Freeze-thaw conditioning machine

The dynamic modulus of prismatic samples was evaluated at every 30 cycles using the transverse frequency test. The dynamic modulus test is an impact test method to measure the transverse frequency. The relative dynamic modulus is then computed using the fundamental transverse frequencies at 0 cycle and the certain number of freeze-thaw cycles. Figure 4.10 shows the test setup for dynamic modulus measurement. The dynamic modulus of the concrete beam samples at different cycles (up to 600 freeze-thaw cycles) were compiled and compared. The decrease of the dynamic modulus over the accelerated freeze-thaw cyclic conditioning indicates the degradation of concrete materials. For example, it is not recommended that samples be continued in the test after their relative dynamic modulus of elasticity has fallen below 60%.

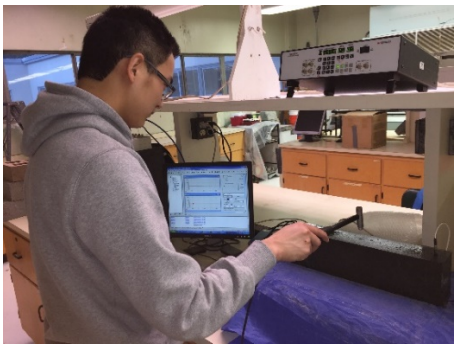

Figure 4.10 Dynamic modulus test setup at WSU

4.4 Pullout tests of UHPC

The considered maximum joint width is to be 11 inch (with 10 inch bar projections from either the double bulb tee (DBT) girders), and smaller joints are preferred. The 11 inch width arises from a 5 ft. girder spacing and a flange width of 49 inch (which corresponds to the sloping part of the flange in a standard DBT). Bars projecting from the flanges will be offset to avoid conflicts during erection, so the lap splices between them will necessarily be non-contact splices, as shown in Figure 4.11. Under these circumstances, the use of larger bars at larger spacing exacerbates the effect of the non-contact characteristic of the splice.

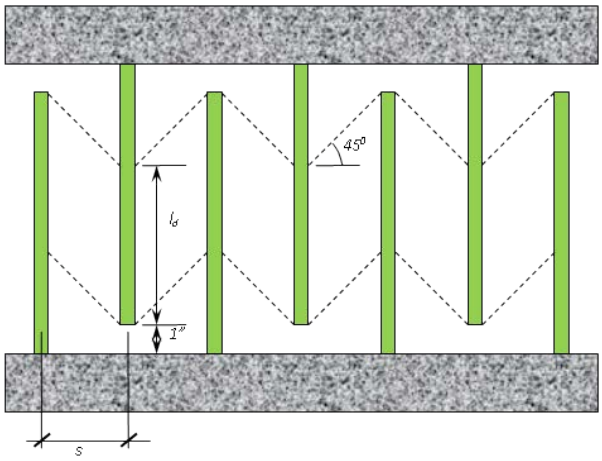

Figure 4.11 Plan view of joint showing available development length for a non-contact splice

Figure 4.12 provides the relationships between bar size, spacing and development length. In Figure 4.12, the arrows show the consequences of choosing a 10 inch wide joint with No. 5 bars at 6 inch spacing projecting from each flange. The assumption of a 45° strut between the bars of the non-contact splice and 1 inch clear between the end of the projecting bar and the face of the adjacent DBT flange leads to an available l_d of 5 inch (see Figure 4.12a), which is shown to be 8 bar diameter (see Figure 4.12b). This could most likely be achieved. However, a relatively small change has a large effect on the outcome. For example, an 8 inch wide joint containing No. 6 bars at 8 inch spacing would require development in 2 inch, or 2.67 bar diameter. This is likely to be challenging. Small bars at small spacing can alleviate the anchorage problem but make the system more prone to bar conflicts during erection, and vice versa. The optimum joint design must balance these objectives.

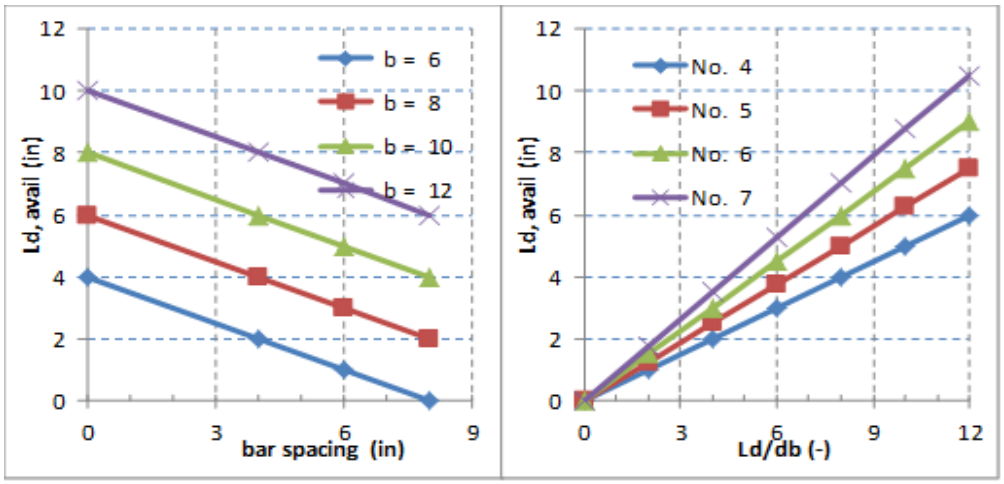

Figure 4.12 Relationships between bar size, spacing and development length

The nature of any bond failure must also be considered. If failure occurs by pullout of bars without edge splitting, as may occur if the available development length is very short and the cover is large, it will be followed by tension failure of the UHPC along diagonal lines as shown in Figure 4.11. However, the system strength in this failure mode could be

increased by placing supplementary reinforcement across the potential diagonal crack. This is more likely to be necessary in narrow joints.

A second failure mode is possible, namely by surface splitting of the concrete and consequent loss of bond. This is especially likely if the cover is small or the distance between adjacent bars is small. The bottom layer of reinforcement will then be critical because the bottom bars may be larger than the top ones and a wearing course will be overlain on the deck, thereby providing additional top cover. Possible solutions include: modifying the UHPC mix to provide greater tensile strength; increasing the bottom cover (but this reduces the lever arm and thus the flexural stiffness and strength); bending the ends of the projecting bars into the slab slightly so that the cover at the bar tip is greater; providing supplementary transverse reinforcement such as hairpins (adds site labor costs and reduces cover), etc.

Pullout tests were conducted at the age of 7 days in this study to determine the bond strength between rebar and UHPC. The No. 5 epoxy-coated rebar Grade 60 was selected as the testing bar, and the No. 8 bar was casted for connecting with the base of testing machine. Two parameters were evaluated for their effects on the bond strength: embedment length and side cover (Table 4.2). Figure 4.13 shows the casting and curing procedures of pullout tests specimens. The pullout tests were conducted under a constant displacement rate of 0.2 in/min and a linear variable differential transformer (LVDT) was used to measure the displacement of rebar. Figure 4.14 shows the schematic and setup of pullout tests.

Table 4.2 Information of pullout (bond strength) tests

Parameters	Information
Bar Type	No. 5 epoxy-coated rebar G60, d_b = 5/8”
Bar spacing, in.	7
Side cover (s_c), in.	1, 2
Embedment Length (l_d), in. (times of d_b)	5, 6.25, 7.5, 8.75 (8, 10, 12, 14)
Age	7 days after casting
Curing condition	Cover with wet burlap followed by plastic sheet, and rewet specimens everyday

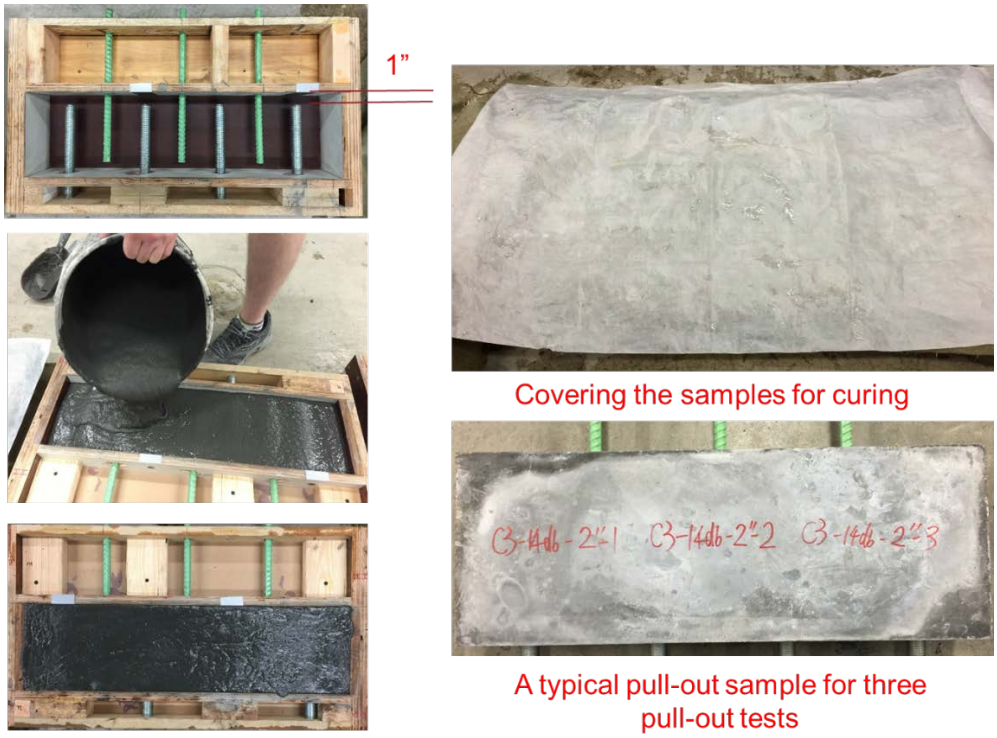

Figure 4.13 Casting and curing procedures of pullout specimens

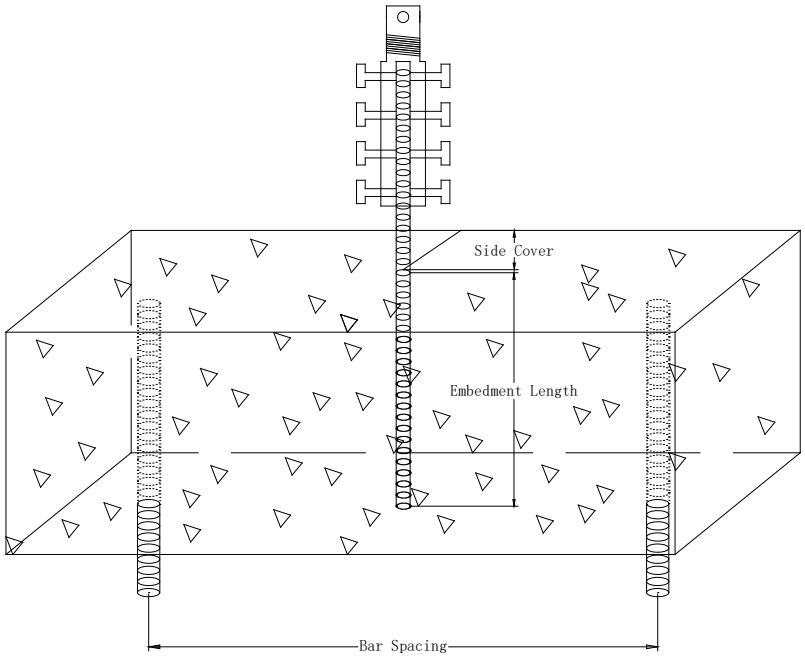

(a) Illustration of pullout tests

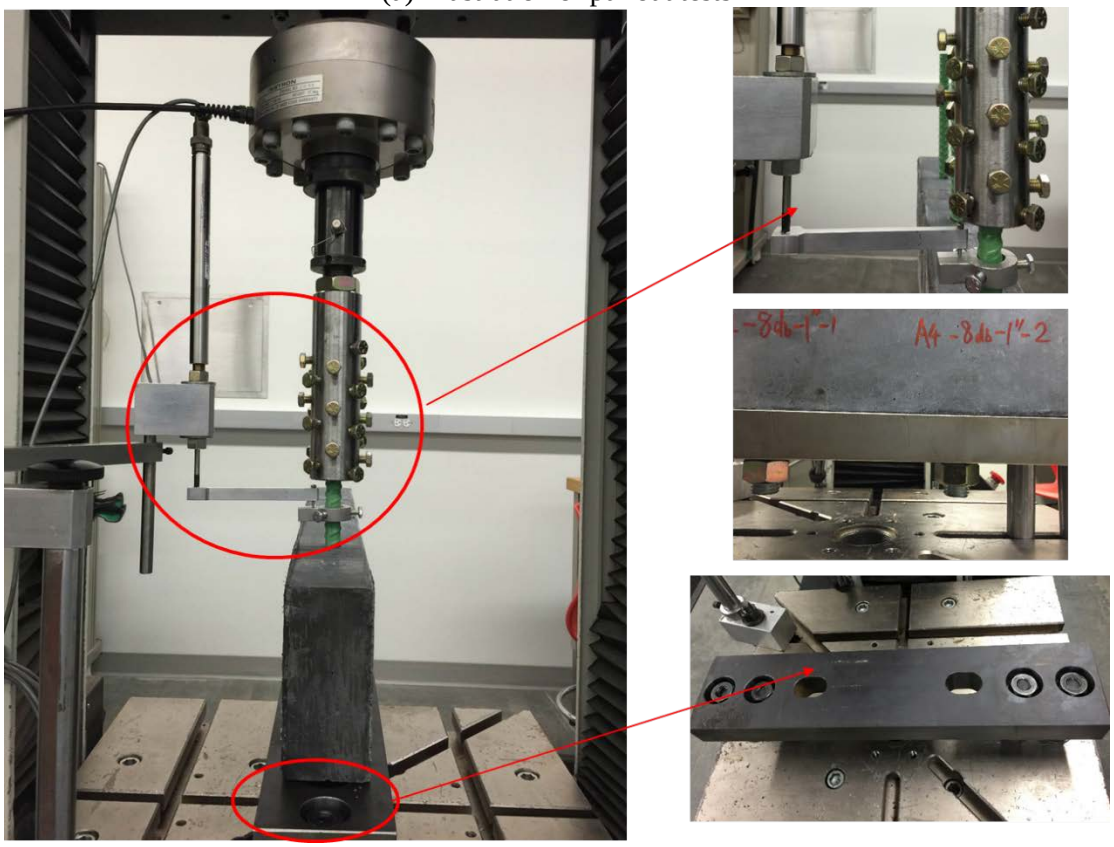

(b) Testing setup

Figure 4.14 Pullout testing illustration and setup

Chapter 5 TEST RESULTS AND ANALYSIS

In this chapter, results from the tests conducted on UHPC specimens are presented and analyzed.

5.1 Results of Fresh and Hardened UHPC

5.1.1 Flow tests

The flow tests were conducted immediately to evaluate the workability after mixing of fresh UHPC. Initially, 12 mix designs (see Table 3.4) with different w/cm ratios, silica fume and cement contents, and HRWRA dosages were tested for their workability. Primarily based on their workability (i.e., the spread diameter from the flow tests, see Table 3.4), two mix designs A4 and C3 which have a spread diameter of more than 8 inch were selected for other mechanical property tests. The average flow for the A4 and C3 are listed in Table 5.1. Both average flow of A4 and C3 is higher than 9 inches in diameter, and the flow of A4 is slightly lower than that of C3. It should be mentioned that the w/c ratio of C3 is lower than that of A4, and thus, a higher dosage of HRWRA was added for compensating its flowability.

Table 5.1 Flow of fresh UHPC

Mixtures	Flow (in.)	w/cm	Dosage of HRWRA
A4	9.0	0.21	7
C3	9.5	0.18	11.5

5.1.2 Compressive strength and modulus of elasticity

The compressive strength and modulus of elasticity for both mixtures of A4 and C3 were measured at 7 days, 14 days, and 28 days to study age-dependent compressive

behaviors. In addition, the geometries of specimen (2 inch cubes, 4 inch cubes, and 4 inch x 8 inch cylinders, respectively) were chosen to evaluate the shape and size effects on the compressive strength. Three replicates were tested for all tests. The averaged test data for the compressive strength and modulus of elasticity are shown in Table 5.2 and Table 5.2 .

Table 5.2 Compressive strength of UHPC (unit: ksi)

Specimen	Age	A4	STDEV	COV	C3	STDEV	COV
2 inch cubes	7	10.41	1.56	15%	11.07	0.52	5%
	14	13.45	1.14	8%	13.78	0.45	3%
	28	14.10	0.40	3%	16.01	0.97	6%
4 inch cubes	7	10.37	0.87	8%	10.97	0.41	4%
	14	12.52	0.34	3%	12.84	0.23	2%
	28	13.37	0.54	4%	14.38	0.34	2%
4 inch x 8 inch cylinder	7	10.26	0.14	1%	10.86	0.37	3%
	14	12.71	0.18	1%	12.59	0.28	2%
	28	13.62	0.80	6%	14.11	0.39	3%

Table 5.3 Modulus of elasticity of UHPC (unit: ksi)

Specimen	Age	A4	STDEV	COV	C3	STDEV	COV
6 inch x12 inch cylinder	7	3657	129	4%	4356	276	65
	14	3819	275	7%	4571	342	7%
	28	4025	82	2%	4882	290	6%

5.1.2.1 Compressive strength

The compressive strength of 2 inch cubes was considered as the reference parameter (benchmark) in this study. Table 5.2 plots the averaged test data for the compressive strength of A4 and C3, and the corresponding compressive strengths at the reference age of 28 days are 14.01 ksi with a standard deviation of 0.4 ksi and 16.01 ksi with a standard

deviation of 0.97 ksi for A4 and C3, respectively. Figure 5.1 indicates that C3, with a lower w/cm ratio, has a higher compressive strength than that of A4. It is also shown that the compressive strength of UHPC rapidly gained after casting, and approximately 75% and 90% of the compressive strength of 28 days were achieved after curing of 7 days and 14 days, respectively.

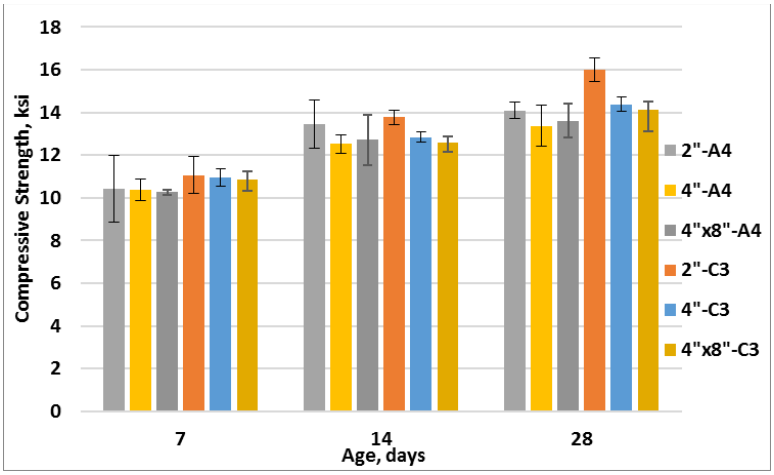

Figure 5.1 Comparison of compressive strengths at different ages and by different size specimens

5.1.2.2 Size effects on compressive strength

Table 5.2 shows that the size of testing specimens has a significant effect on the compressive strength of UHPC. Again, the compressive strengths of 2 inch cubes were set as the reference data. It can be observed that the 2 inch cubes exhibited greatest compressive strength, while the compressive strengths of 4 inch cubes were almost the same as those of 4 inch x 8 inch cylinders. The strength ratios decreased with the increasing ages. As shown in Figure 5.2, the 4 inch cubes and the 4 inch x 8 inch cylinders almost have the same compressive strengths at the different age, and the 4 inch cubes and the 4 inch x 8 inch cylinders produced from A4 mixture have approximately 99%, 94%, 95% of 2 inch cubes at 7 days, 14 days and 28 days, respectively. Similarly, the 4 inch cubes and 4

inch x 8 inch cylinders produced from C3 mixture have about 99%, 92%, 89% of 2 inch cubes at 7 days, 14 days and 28 days, respectively. The possible reason can be attributed to that the relative larger specimens take longer time for the water absorption or diffusion inside, which is related to the hydration of cementitious materials of UHPC. Also, it can be attributed to the fact that the concrete is composed of elements of variable strength and when a larger volume of concrete is subjected to a uniform stress, it is more likely to contain a weaker element and subsequently early failure leading to lower strength.

Figure 5.1 also shows that the smaller cubes usually have larger standard deviation because air bubbles inside UHPC were relatively difficult to come to the surface during the vibration. Similar phenomena were observed by Orgass and Klug (2004) and Graybeal (2006).

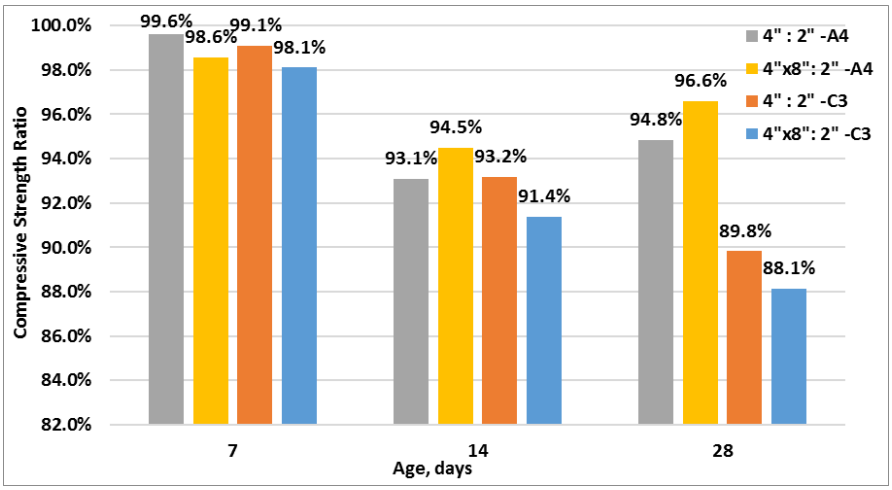

Figure 5.2 Size effects on compressive strength

5.1.2.3 Relationship between modulus of elasticity and compressive strength

The modulus of elasticity of concrete generally shows some correlation with its compressive strength. The ACI committee 318 (2014) provides one of the most widely used relationship for normal concrete, i.e., the modulus of elasticity equals to a constant multiplied by the square root of the compressive strength, which can be expressed by

$$E = \alpha\sqrt{f_c'} \tag{5.1}$$

where: E - modulus of elasticity, ksi;

f_c' - compressive strength, psi;

α - scale factor.

Following Eq. (5.1), the test data presented in Table 5.2 and Table 5.2 were used to find the empirical relationships between the modulus of elasticity and its compressive strength. The scalar factors in Eq. (5.1) were determined from the least square method, resulting in α = 36,000 and 41,000 for A4 and C3, respectively. As shown in Figure 5.3, the modulus of elasticity prediction equation can accurately fit the curve from the experimental results. Due to greater compressive strength of UHPC, the scale factors for A4 and C3 in Eq. (5.1) are smaller than that of conventional concrete of normal weight (α = 57,000).

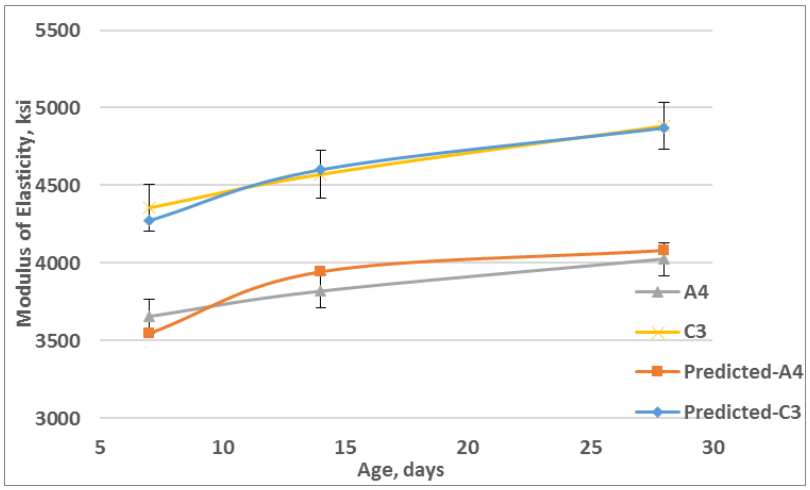

Figure 5.3 Comparison of modulus of elasticity between the measured and predicted values

5.1.3 Tensile strength

Three test methods were employed to measure the tensile strength-associated properties of UHPC: (1) flexural prisms with dimensions of 3 inch x 4 inch x 16 inch, (2)

splitting cylinders of 6 inch x 12 inch, and (3) direct tensile dogbones with cross section of 2 inch x 2 inch. Tensile strength tests were also conducted at 7 days, 14 days and 28 days to study the tensile strength development over time. The averaged testing results for the flexural strength (MOR: modulus of rupture), splitting tensile strength (ST), and direct tensile strength (DT) are shown in Table 5.2 , where the peak loads were used for the calculation.

Table 5.4 Tensile strength of UHPC by different test methods (unit: ksi)

Specimen	Age	A4	STDEV	COV	C3	STDEV	COV
3”x4”x16” Prism	7	1.55	0.18	12%	2.33	0.03	1%
	14	2.24	0.24	11%	2.37	0.35	15%
	28	2.67	0.08	8%	2.72	0.37	14%
6”x12” Cylinder	7	1.46	0.12	8%	1.12	0.12	10%
	14	1.51	0.12	8%	1.18	0.17	14%
	28	1.56	0.21	13%	1.23	0.07	6%
2”x2” cross section; 6” gage length	7	0.74	0.03	3%	1.06	0.04	4%
	14	0.78	0.10	13%	1.21	0.05	4%
	28	0.91	0.07	8%	1.19	0.14	12%

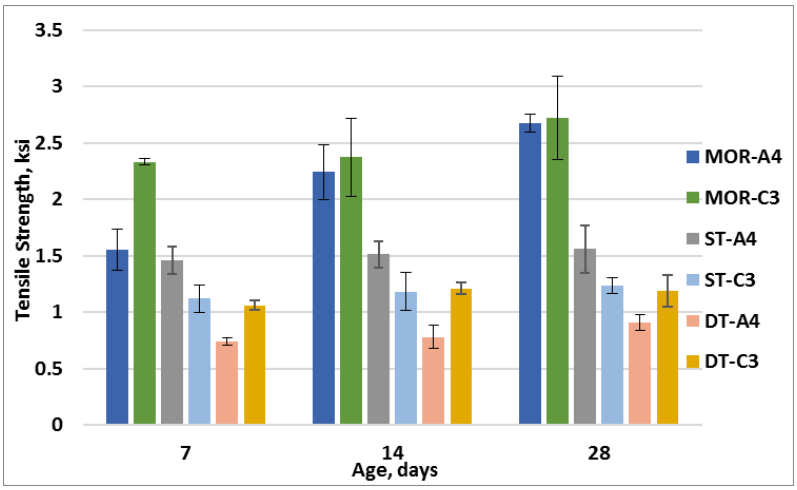

Figure 5.4 Comparison of tensile strength

Figure 5.4 presents the tensile strength of UHPC from three different approaches mentioned above, and the values from them, though they are different, are all much higher than those of conventional concrete. The tensile strength of C3 at all ages from splitting cylinders and dogbones were greater than those of A4; while the flexural beams showed the opposite result. Among three different approaches for measuring the tensile strength, the flexural strength test reported the greatest (2.6 ksi at 28 days), followed by splitting tensile strength (1.5 ksi at 28 days) and direct tensile strength (1.0 ksi at 28 days). The significant difference in tensile strength values measured by these three test methods may be caused by the overestimation of the tensile hardening response and different stress distributions and boundary conditions in the test specimens. In general, UHPC can exhibit sustained strain hardening and then reach greater tensile strength after first cracking. It has been observed that the flexural beam- and splitting cylinder-based test methods are more susceptible to overestimation of tensile load due to the tensile strength at peak load after post-cracking can even be 3 times of tensile load at first cracking (Graybeal 2013). The boundary conditions and load applications cause nonuniform tensile stress distribution in the test specimens (e.g., the linear stress distribution through the depth of the beam in the flexural beams and stress concentrations at the loading points and nonuniform stress distribution in splitting cylinders). However, the peak post-cracking tensile strength in the direct tension test just showed slightly greater than that at the first cracking, and the tensile stress distribution in the cross section of direct tension is much uniform compared to those of flexural beams and splitting cylinders. In addition, due to the limited tests being conducted, the strain responses in flexural beams and splitting cylinders were not measured, and the stress-strain curve and the tensile load at first cracking could not be observed.

An extensometer with 2 inch gauge length was used to monitor the responding tensile strain at the middle of the specimens in the direct tension tests. Since the dogbones had a gage length of 6 inch in the middle while the gage length of extensometer was only 2 inch, the cracking occurred within the gage length of extensometer at a relatively low probability. More direct tension tests with LVDTs of sufficient gage length are needed for further study. Figure 5.5 showed the stress-strain relationship curves in direct tension tests. The full stress-strain response curves could be obtained if the cracking occurred within the gage length of extensometer; while only the elastic phase till the first cracking was shown if it occurred out of the 2 inch extensometer measuring range (see Figure 5.5).

It can be seen from Figure 5.5 that the stress-strain response and failure mode of UHPC in direct tension were greatly different from those of conventional concrete. UHPC exhibited excellent ductile behavior with gradual decline in the stress versus the strain due to the reinforcement of steel fibers. This ductile response can be divided into four phases. Phase I is the linear elastic behavior which is from the initial load application until the first crack occurs. Phase II shows that no stress falling branch and multiple cracks form strain hardening. Next, in Phase III, gradual decrease in the stress versus the strain due to pullout of steel fibers. In Phase IV, after onset of cracks, it shows stress-crack opening behavior (strain softening). The strain at the first crack is ranged from 0.015% to 0.025%, but it showed no clear relationship with the age of testing in this study. The post cracking occurred near the strain of 0.3%. The UHPC can possess more than 50% of tensile strength when the tensile strain has reach 3%.

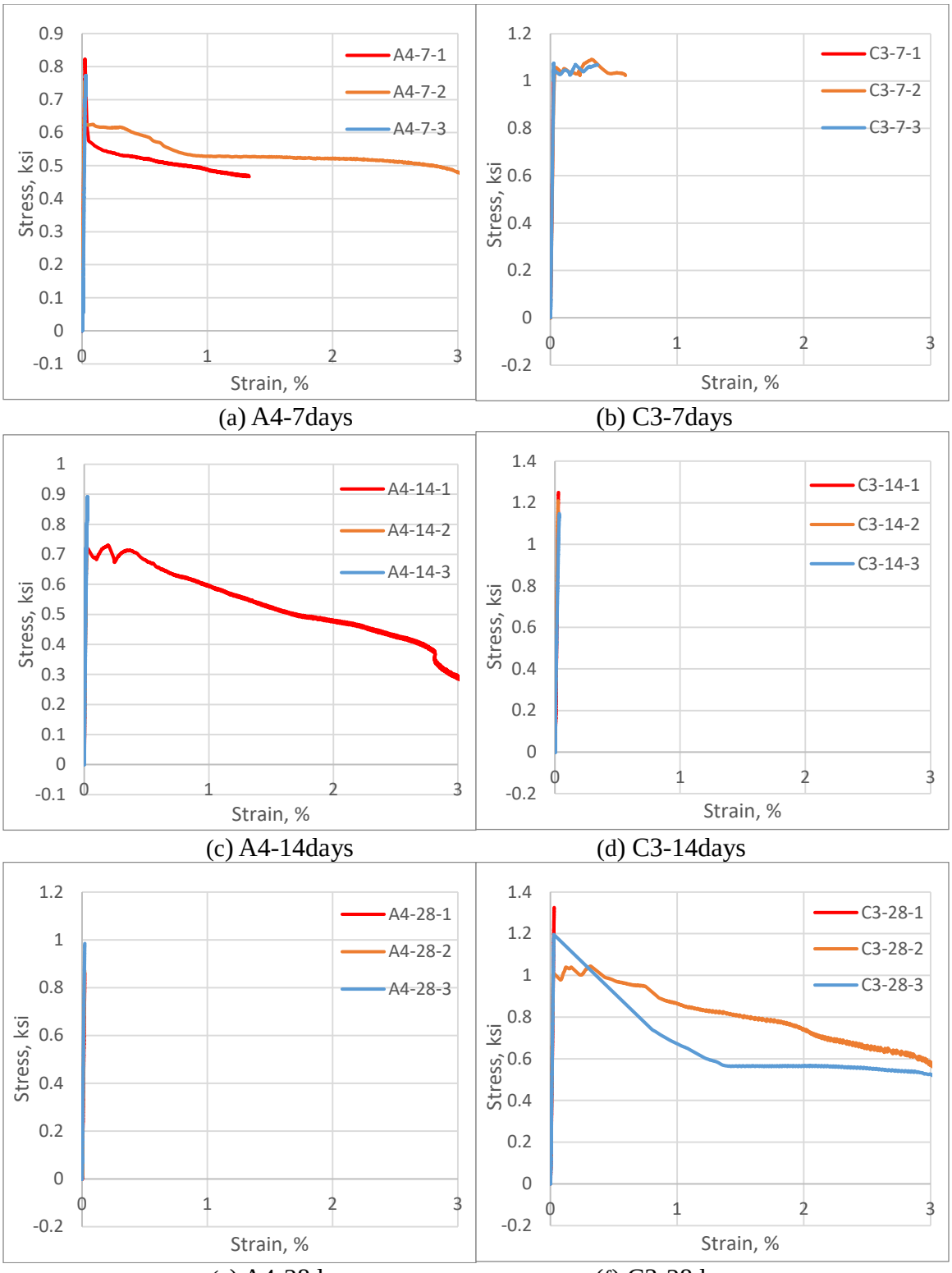

(a) A4-7days (b) C3-7days

(c) A4-14days (d) C3-14days

(e) A4-28days (f) C3-28days

Figure 5.5 Stress-strain response of UHPC in direct tension

An alternative method to obtain the modulus of elasticity is to find the slope of elastic

domain from the stress-strain relationship curves obtained from the direct tension test. The averaged moduli of elasticity from direct tensile strength (DT) of C3 and A4 at different ages are shown in Table 5.2 . The comparison with the results from the 6 inch x12 inch cylinder compression tests are shown in Figure 5.6. The difference between the modulus of elasticity values obtained from the direct tension and cylinder compression tests is approximately 5%.

Table 5.5 Modulus of elasticity of UHPC from direct tensile test (unit: ksi)

Specimen	Age	A4	STDEV	COV	C3	STDEV	COV
2”x2” cross section; 6” gage length	7	3536	149	4%	4078	284	7%
	14	4300	292	7%	4275	630	15%
	28	4398	266	6%	4564	164	4%

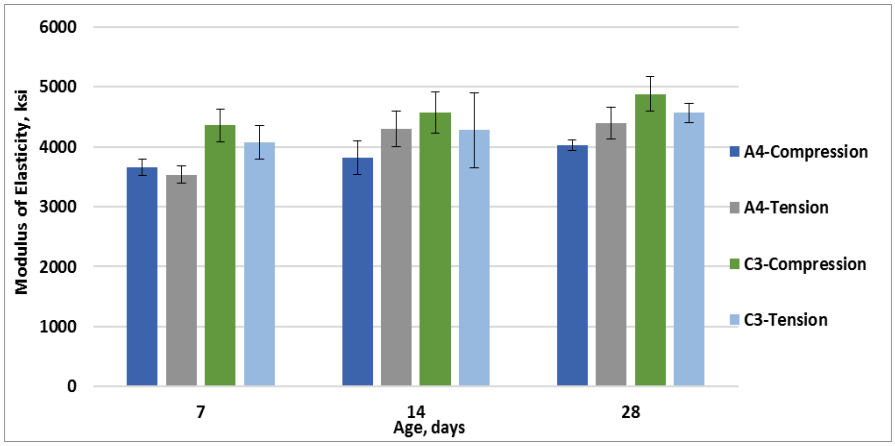

Figure 5.6 Comparisons of modulus of elasticity

5.1.4 Shrinkage

Shrinkage of unstrained UHPC prismatic specimens were measured from the demolding until 28 days. Prismatic specimens of sizes of both 1 x 1 x 11.25 inch and 4 x 4 x 11.25 inch were used to investigate the size (specific surface to volume ratio) effects on shrinkage. All prisms were stored, and initial lengths were measured in a climate controlled

room with temperature of 73±3°F (23±2°C) and relative humidity of 50±4%. The only difference was the surface treatment: sealed surface for autogenous shrinkage and unsealed for free shrinkage.

Figure 5.7 depicts the autogenous shrinkage behavior of UHPC specimens up to 28 days after demolding and lists the average values at 7 days, 14 days and 28 days. The cross sections of prisms have great effect on the autogenous shrinkage behavior of UHPC due to different moisture diffusion distance. For both the tested mixtures (i.e., A4 and C3), the 1 inch prisms showed greater autogenous shrinkage and faster shrinkage rate than those of 4 inch prisms. The mixture of C3 with 1 inch cross section exhibited much greater autogenous shrinkage than A4, while C3 with 4 inch cross section only showed slightly greater autogenous shrinkage than A4. It should be mentioned that from the inherent relationship among hydration of cementitious materials, autogenous shrinkage and strength growth, 4 inch prisms were more representative and consistently matched the strength gain rate better than 1 inch slimmer prisms for shrinkage measurement. Though C3 had lower w/cm ratio, it still showed a litter higher autogenous shrinkage. A possible reason could be the addition of HRWRA, which also contains some water in C3.

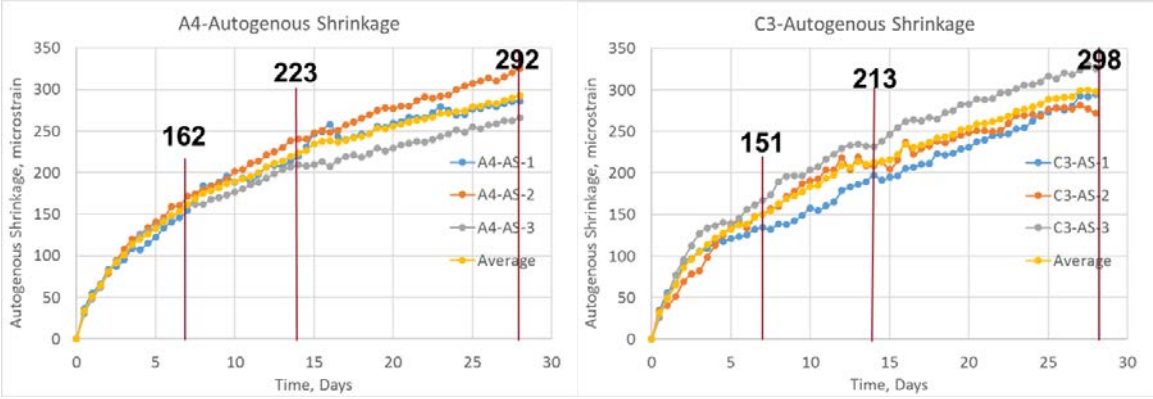

(a) A4-Autogenous shrinkage-4" prisms (b) C3-Autogenous shrinkage-4" prisms

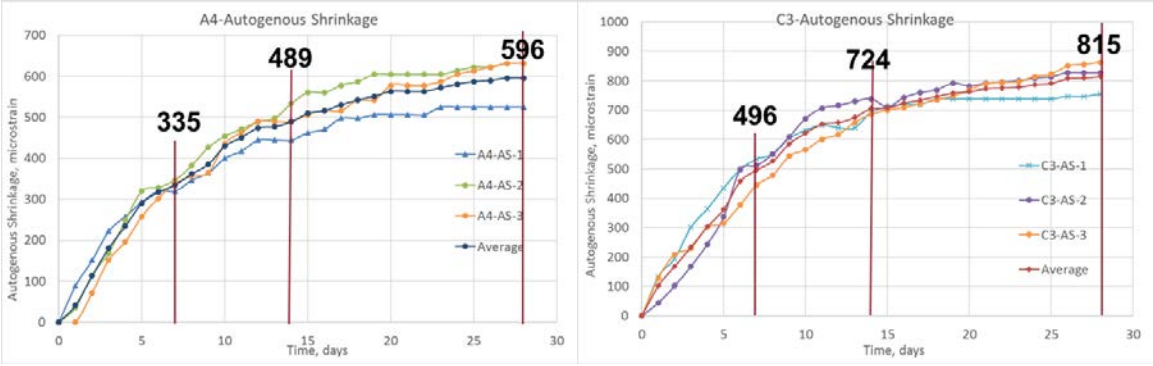

(c) A4-Autogenous shrinkage-1" prisms (d) C3-Autogenous shrinkage-1" prisms

Figure 5.7 Comparison of autogenous shrinkage

Figure 5.8 provides the free shrinkage of UHPC mixtures up to 28 days after demolding. Free shrinkage mainly consists of both autogenous shrinkage and drying shrinkage. After 28 days of exposure to 50% RH, the average shrinkage values for A4 and C3 were 653 and 678 microstrains, respectively. It can be seen that the free shrinkage behavior showed similar trend of autogenous shrinkage. For both mixtures, the 4 inch prisms showed much less and slower free shrinkage than those of 1 inch prisms, and approximately 90% of free shrinkage for 1 inch prisms occurred after 7 days. The C3 mixture exhibited slightly greater shrinkage values and shrinkage rate than those of A4, though C3 had lower w/cm ratio. Again, the possible reason could be attributed to the influence of additional water from HRWRA in C3.

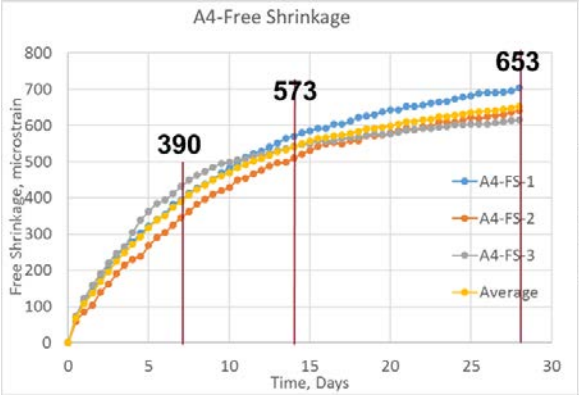

(a) A4-Free shrinkage-4" prisms

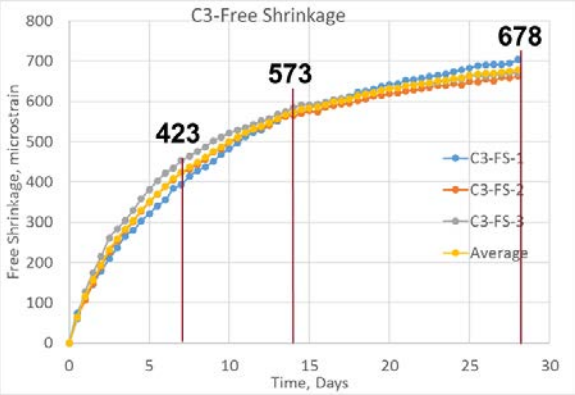

(b) C3-Free shrinkage-4" prisms

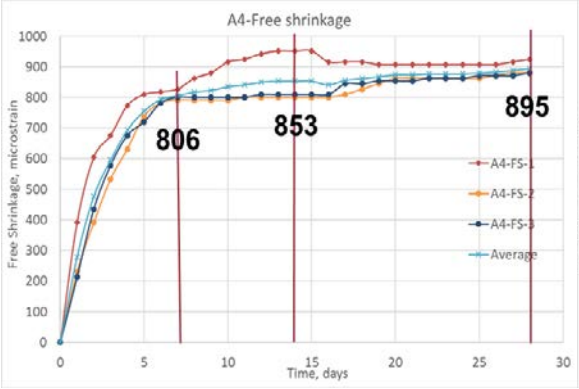

(d) A4-Free shrinkage-1" prisms

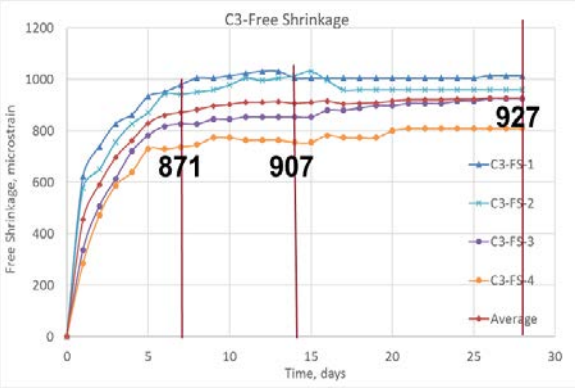

(d) C3-Free shrinkage-1" prisms

Figure 5.8 Comparison of free shrinkage

Figure 5.9 depicts the testing results of restrained shrinkage performed on both mixtures of UHPC used in this study, and it shows the measured steel strains in the restrained ring specimens. No sudden jump (usually happens in case of conventional concrete within 28 days) is observed in these shrinkage strain curves, indicating no shrinkage-induced cracking occurs in the ring. It can also be seen from Figure 5.9 that A4 demonstrates greater strain in the insider steel ring than C3 after 28 days drying. As aforementioned, A4 and C3 present comparable performance in both autogenous shrinkage and free shrinkage, but the results are actually measured after the first day of curing. Figure 5.9 shows the difference of autogenous shrinkage at the first day after casting, i.e., 41 and 22 microstrains for A4 and C3, respectively. After deducting these initial values from the steel strains, the remained steel strains from the first day are closer, i.e., 152 and 147

microstrains for A4 and C3, respectively.

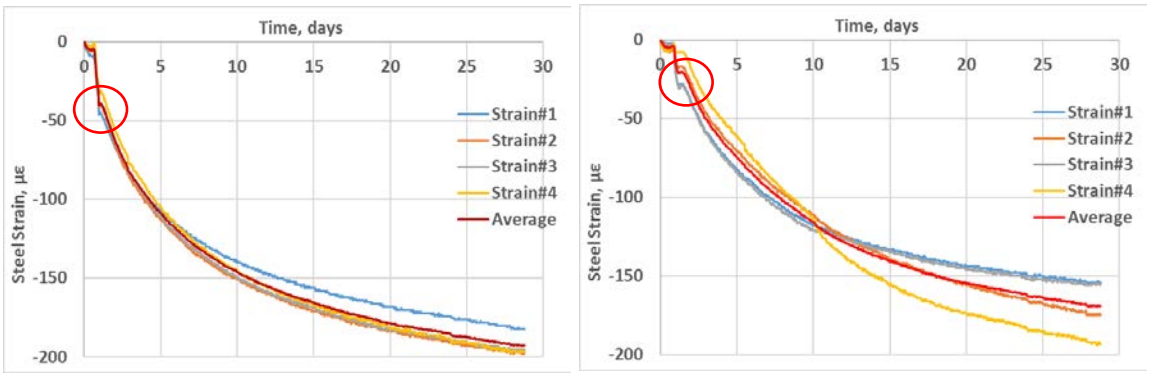

(a) UHPC mixture A4 (b) UHPC mixture C3

Figure 5.9 Comparison of restrained shrinkage from ring tests

5.1.5 Dynamic modulus

The vibration-based dynamic modulus (E_{dyn}) test using impact hammer was conducted on the control groups of UHPC beams during the curing period up to 90 days. The average dynamic modulus and modulus of elasticity (MOE) from the compressive test with respect to the curing age are comparatively illustrated in Figure 5.10. It can be seen from Figure 5.10 that the modulus obtained from both test methods gradually increase with the increasing of the curing time, indicating that the samples are gradually gaining stiffness and strength. The modulus of elasticity of concrete is influenced by the loading rate, modulus of elasticity by compressive test is obtained under quasi-static loading while the dynamic modulus is based on low frequency (1-10 kHz). Thus, the dynamic modulus is higher than the modulus of elasticity.

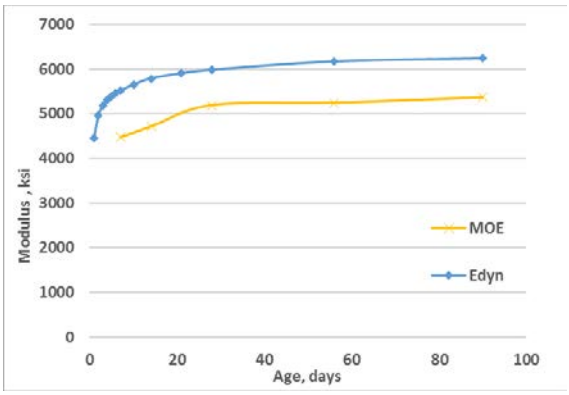

Figure 5.10 Comparison of modulus of elasticity

In parallel, the aforementioned non-destructive monitoring technique, vibration-based dynamic modulus (E_{dyn}) tests were simultaneously conducted on UHPC beams at different freeze-thaw (F-T) conditioning cycles. In the meantime, the control groups of UHPC beams continue to be kept under lime-saturated water. The average dynamic modulus with respect to the curing cycles are comparatively illustrated in Figure 4.11. UHPC beams were conditioned up to 600 freeze-thaw cycles due to time limit. As seen in Figure 4.11, the dynamic modulus values increase instead of decreasing with the increasing of freeze-thaw cycles, which is different from that of normal concrete but similar to others' conclusions (Graybeal and Hartmann, 2003; Shaheen and Shrive, 2006), indicating that UHPC exhibits excellent frost resistance at first 600 cycles. The maximum increased ratio of dynamic modulus with freeze-thaw conditioning is 5.2%. In comparison, the maximum increased ratio of dynamic modulus in the control group is 13.9%. Two possible reasons are considered to explain the difference: (1) the cement hydration with external moisture supply outpaces the frost damage; (2) the cement hydration slows down at lower temperatures. Thus, the experimental evaluation tests will be conducted on UHPC beams with more freeze-thaw cycles (up to 1,500 cycles) in future study, and microstructure study on conditioned UHPC will be conducted to reveal the frost damage forming mechanism.

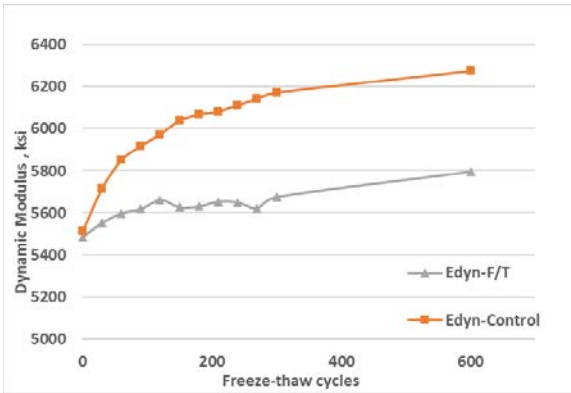

(a) Comparison of dynamic modulus

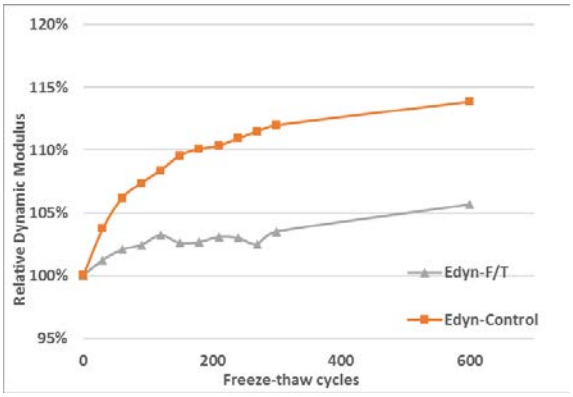

(b) Comparison of relative dynamic modulus

Figure 5.11 Comparison of dynamic modulus values and their relative modulus

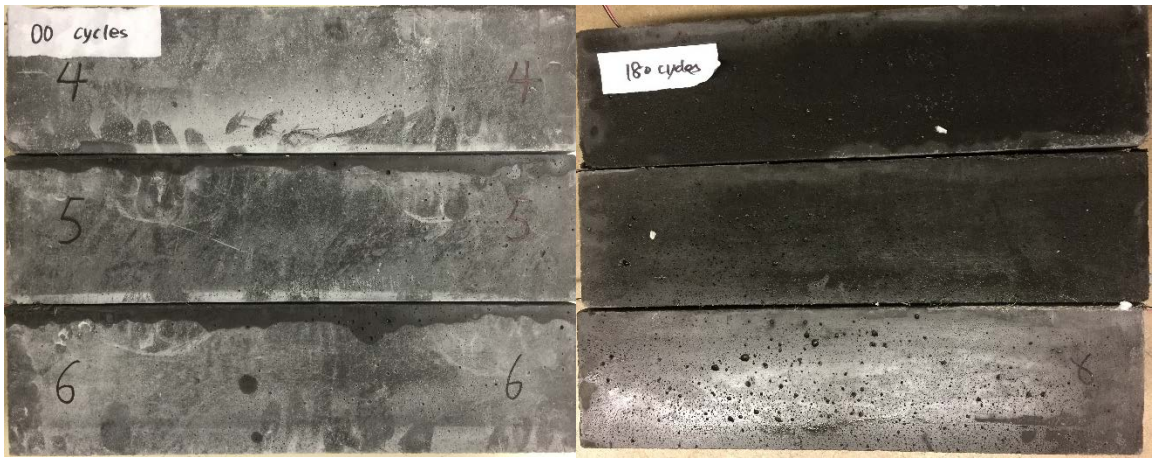

(a) 0 cycles (b) 180 cycles

(c) 300 cycles (d) 600 cycles

Figure 5.12 Comparison of surface scaling of UHPC at different freeze-thaw cycles

The surface scaling of UHPC samples at 0, 180, 300, 600 cycles are illustrated in Figure 5.12. Few tiny scaling spots on the sample surface are observed after 600 cycles due

to the dense micro-structure of UHPC, and thus the effects of surface scaling under freeze-thaw condition are negligible.

5.2 Results of Pullout Tests

Pullout tests for both the mixtures (A4 and C3) were conducted to comparatively investigate the bond performance of deformed reinforcing bar in UHPC, which is essential for connecting the flanges of adjacent deck bulb tees. The No. 5 epoxy-coated Grade 60 rebar was selected as the testing bar, and two parameters were evaluated for their effects on the bond behaviors, i.e., the embedment length of rebar (l_d) and side cover of UHPC (s_c), respectively.

5.2.1 Bond strength

The bar stresses at the first crack and peak loads were both considered to characterize the bond performance of UHPC. The first crack was visibly observed, and some micro cracks were ignored. The peak loading stage was always reached after the occurrence of diagonal and splitting cracks.

The bar stresses are calculated by dividing the first crack and peak loads by the cross section of rebar (Equations 5.1 and 5.2). The corresponding bond strength can be calculated by dividing the bar force by the overall contact area between rebar and UHPC (Equations 5.3 and 5.4) as follows.

Bar stress at first crack: $$\sigma = \frac{4P_{1,crack}}{\pi d_b^2} \quad (5.1)$$

Bar stress at peak load: $$\sigma = \frac{4P_{peak}}{\pi d_b^2} \quad (5.2)$$

Bond strength at first crack: $$\mu = \frac{P_{1,crack}}{\pi d_b l_b} \quad (5.3)$$

Bond strength at peak load: $\mu = \frac{P_{peak}}{\pi d_b l_b}$ (5.4)

where, $P_{1,\,first}$ is the load when the first crack occurs;

P_{peak} is the load at peak;

d_b is the diameter of rebar;

l_d is the embedment length of rebar.

Tables 5.6 and 5.7 provide the test data of bar stresses at the first crack and peak loads for A4 and C3, respectively. Table 5.8 lists the corresponding bond strength determined from the bar stress.

Table 5.6 Bar stress of A4 from pullout tests (unit: ksi)

A4	l_d/d_b	@ First Crack	STDEV	COV	@ Peak Load	STDEV	COV
1” Side cover	8	34.18	0.75	2.2%	34.18	0.75	2.2%
	10	46.55	0.96	2.1%	46.55	0.96	2.1%
	12	54.29	9.82	18.9%	62.42	9.65	15.5%
	14	55.64	9.27	16.7%	62.84	4.90	7.8%
2” Side cover	8	44.84	4.47	5.8%	52.83	4.12	7.8%
	10	65.11	-	-	70.62	-	-
	12	66.09	1.66	2.5%	93.49	1.29	1.4%
	14	75.47	-	-	>94.46*	-	-

**Note: Rebar ruptured instead of being pulled out.*

Table 5.7 Bar stress of C3 from pullout tests (unit: ksi)

C3	l_d/d_b	@ First Crack	STDEV	COV	@ Peak Load	STDEV	COV
1” Side cover	8	32.41	5.53	17.1%	32.88	5.10	15.5%
	10	44.60	4.99	11.2%	46.70	3.47	7.4%
	12	59.03	3.85	6.5%	59.03	3.85	6.5%
	14	56.86	3.45	6.1%	66.40	4.04	6.1%
2” Side cover	8	44.20	1.10	2.5%	44.90	1.27	2.8%
	10	56.98	4.73	8.3%	65.45	6.15	9.4%
	12	66.97	-	-	86.09	-	-
	14	72.61	-	-	>94.46*	-	-

** Note: Rebar ruptured instead of being pulled out.*

Table 5.8 Bond strength from pullout tests (unit: ksi)

Bond Strength	l_d/d_b	A4		C3	
		@ First Crack	@ Peak Load	@ First Crack	@ Peak Load
1” Side cover	8	1.07	1.07	1.01	1.03
	10	1.16	1.16	1.11	1.17
	12	1.13	1.30	1.23	1.23
	14	0.99	1.12	1.01	1.19
2” Side cover	8	1.40	1.65	1.38	1.40
	10	1.63	1.77	1.42	1.64
	12	1.38	1.95	1.40	1.79
	14	1.35	1.69	1.30	1.69

5.2.1.1 Effect of embedment length

The embedment length is a key factor which significantly influences the bond performance of reinforcing bar embedded in UHPC. The effect of embedment length on the bond strength was investigated by keeping other parameters constant and varying the embedment length. The different embedment lengths considered are $8d_b$, $10d_b$, $12d_b$, and

$14d_b$. The bar stresses at failure versus the embedment length is depicted in Figure 5.10.

As shown in Figure 5.13 and expected, the bar stress at failure increases with the increase in embedment length of reinforcing bar. An approximately linear relationship is observed between the bar stress and bond length, similar to the phenomena observed on the embedding rebar in conventional concrete (ACI 408 R-03, 2012). It can be assumed that the bond force is uniformly distributed across the depth of surrounding rebar and all lugs of rebar evenly help bearing the axial tensile force. The bar stress at peak load is equal to or slightly greater than that at the first crack for the rebar with a lower bond length, while it shows much higher difference when a deeper embedment length is present, indicating more strain hardening work and more work energy were generated. In addition, the higher the bar stress it reached, the higher difference it showed. Rebar ruptured instead of being pulled out for the specimen with the bond length of $14d_b$ and the side cover of 2 inch.

As shown in Figure 5.14, the resulting bond strength at failure is fitted with a constant value at varied embedment length of reinforcing bar. Thus, the bond strength is known as an inherent design parameter of UHPC which is independent with the embedment length; but it relates to mix design, bar size/type, side cover, etc.

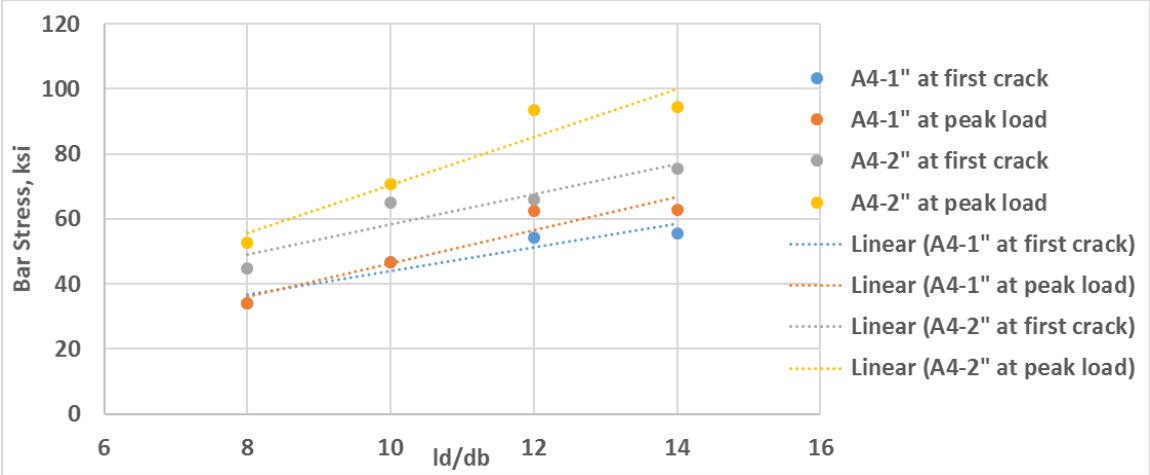

(a) UHPC mixture A4

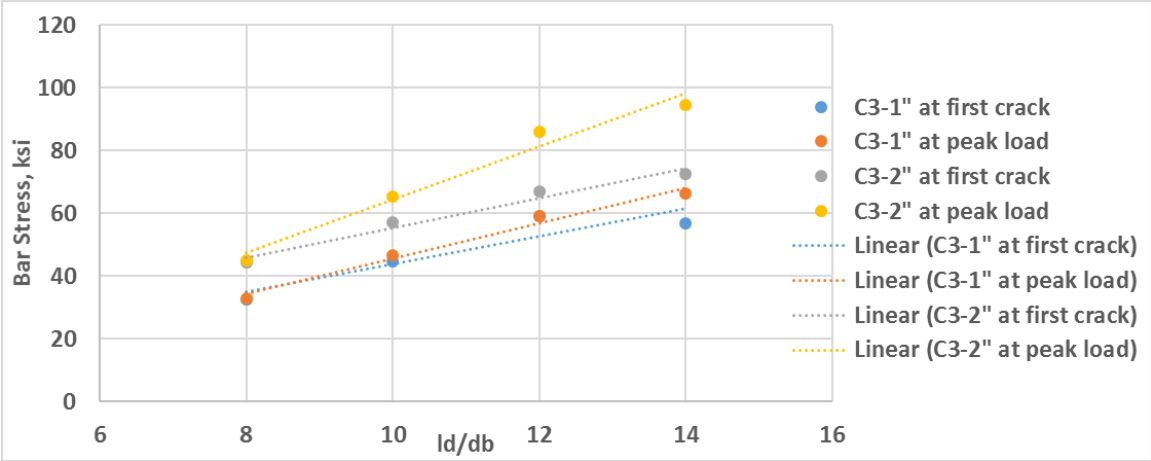

(b) UHPC mixture C3

Figure 5.13 Bar stress at failure under different embedment length

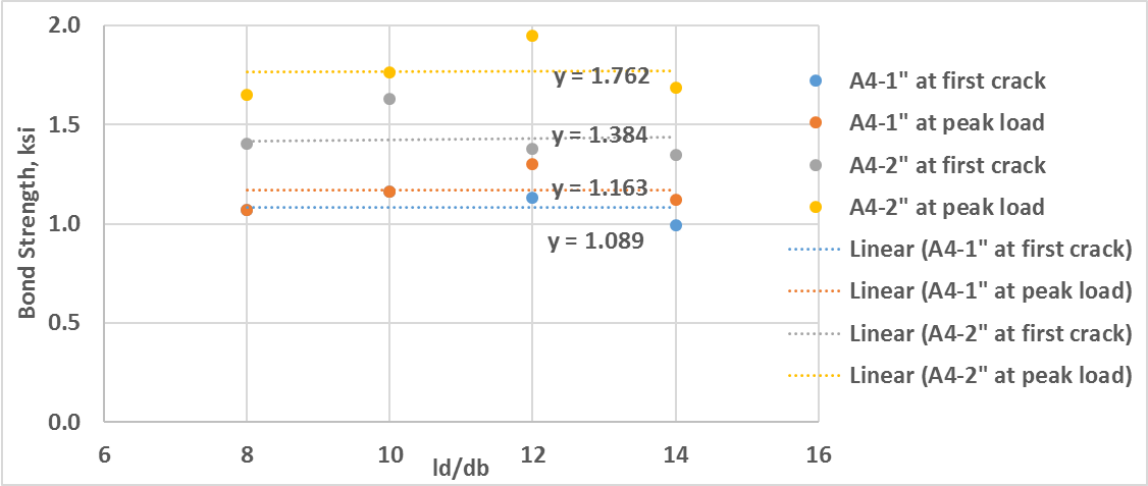

(a) UHPC mixture A4

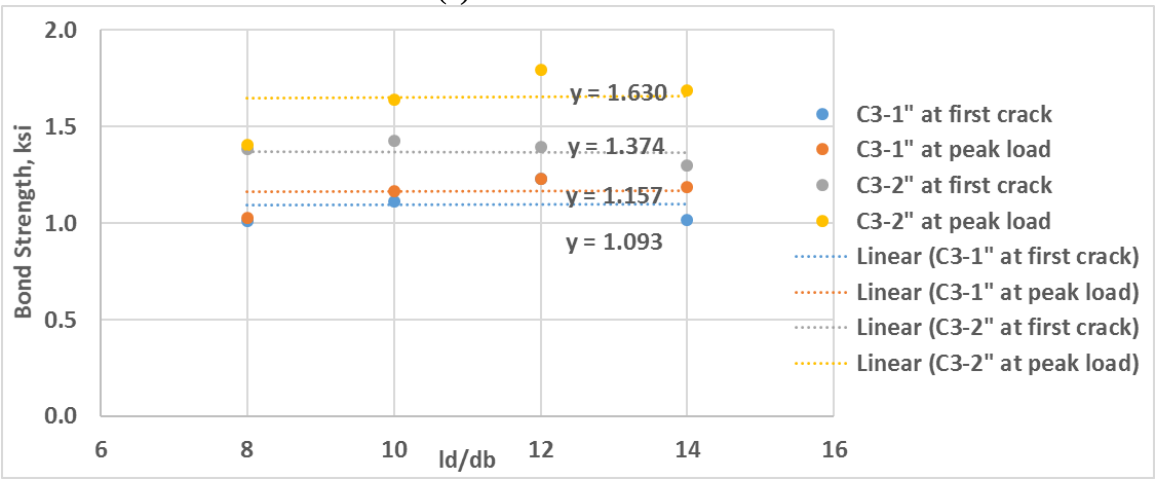

(b) UHPC mixture C3

Figure 5.14 Bond strength at failure under different embedment length

5.2.1.2 Effect of side cover

The side cover is another factor that affects the bond behavior of rebar embedded in UHPC. Based on the practical design parameters considered for the connection joint in deck bulk tees, two typical side covers were considered in the study, i.e., 1 inch (bottom cover) and 2 inch (top cover), respectively. Figures 5.15 and 5.16 show the bar stress at failure and bond strength, respectively. From Equations 5.1 to 5.4, it is known that the bond strength is proportional to the bar stress when only varying the side cover. The rebar with the thicker side cover exhibits higher bond strength since more energy is needed for the cracks to propagate from the bar to the free concrete surface. However, the relationship

between the bond strength and side cover did not show any clear correlations, and the bond strength showed approximately 25% - 50% higher when the side cover increased from 1 inch to 2 inch. Thus, further study regarding the side cover is necessary to systematically investigate its influence on the bond strength.

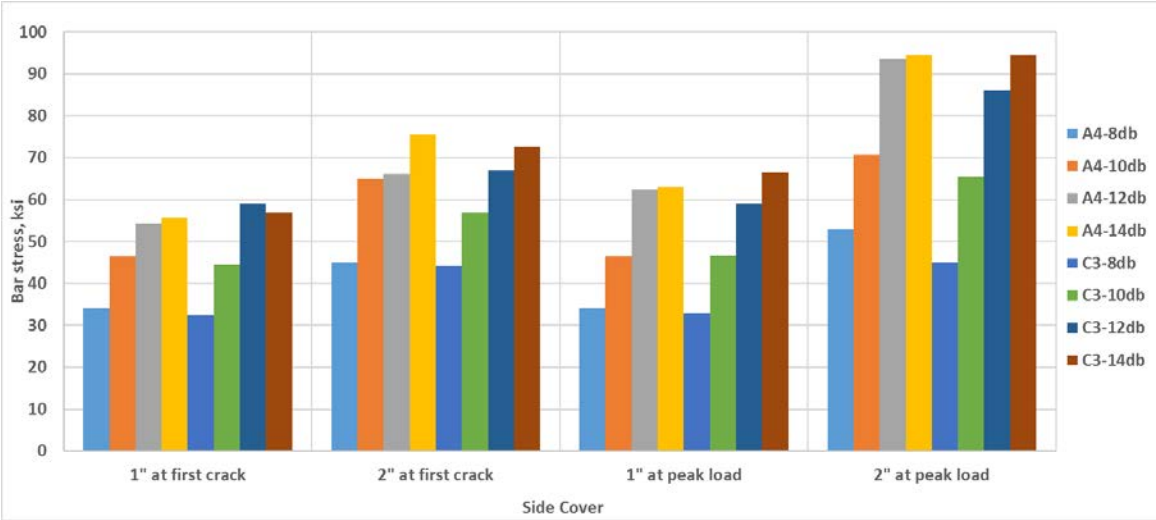

Figure 5.15 Bar stress at failure under different side cover

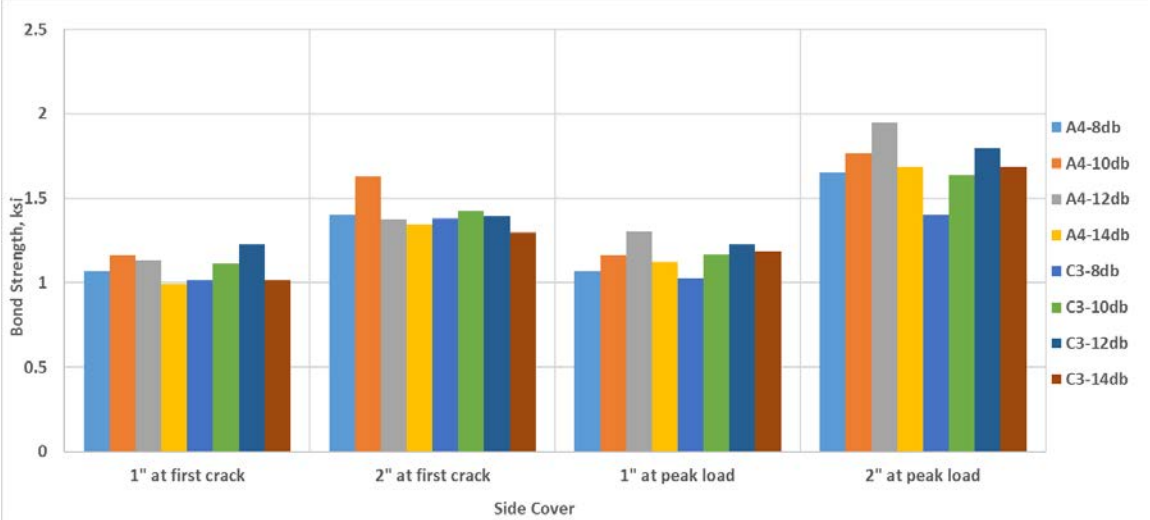

Figure 5.16 Bond strength under different side cover

5.2.1.3 Effect of mixtures

To compare the bond performance between A4 and C3, the testing results in Table 5.8 are plotted in Figure 5.17. As shown in Figure 5.17, for both the side covers, A4 exhibits a little higher bond strength at the peak load than C3, but they have comparable values at the

first crack load. Yuan and Graybeal (2014) investigated the influence of the compressive strength of UHPC on the bond strength by testing the same mix design at different curing ages, and they concluded that the bond strength increased with the increase in compressive strength and the shorter critical embedment length with longer cured period could achieve the required bond. The bond behavior is more related to tensile strength of concrete, which is also related to the compressive strength. Thus, it is reasonable that A4 and C3 had comparable bond strength due to approximately same compressive strengths achieved at 7 days.

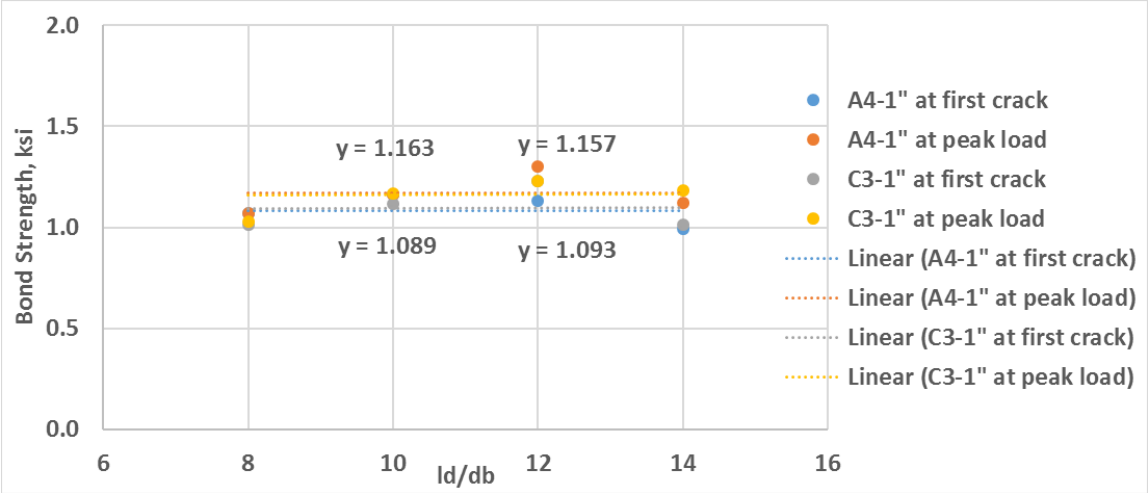

(a) Side cover of 1 inch

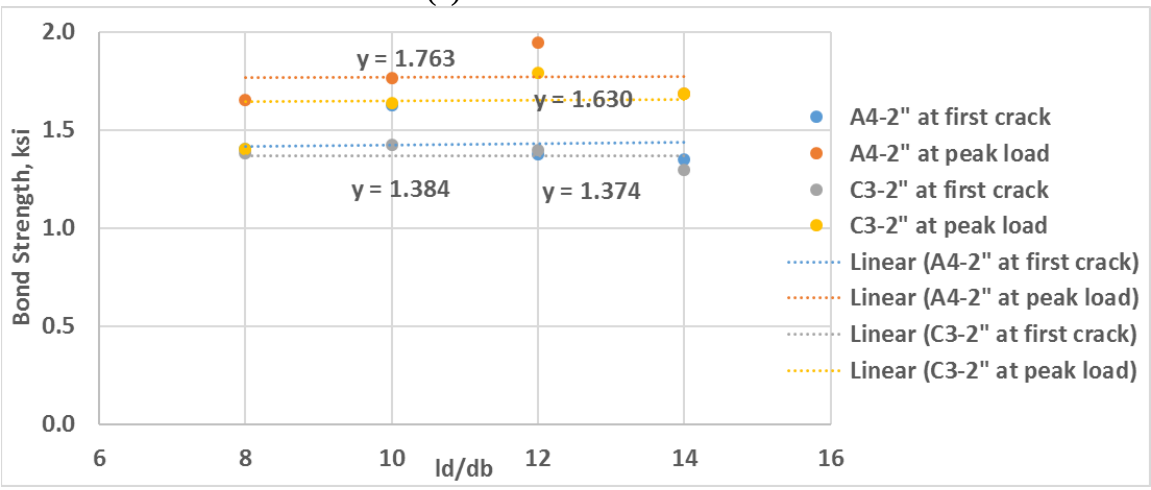

(b) Side cover of 2 inch

Figure 5.17 Comparison of bond strength between two mixtures

5.2.1.4 Critical embedment length

In this study, the critical embedment length is defined as an adequate length when the axial tensile stress attains the allowable yield strength of rebar before concrete cracks and bar slips. Thus, the bar stress at the first crack is employed to evaluate the critical embedment length of UHPC. In addition, from the mechanical testing of epoxy-coated bar Grade 60 of Yuan and Graybeal (2014), the yield strength and tensile strength were found to be 75 ksi and 118 ksi, respectively, but the designed yield strength, 60 ksi, is still used to allow some safety margin. Thus, the critical embedment length is determined by drawing the level line of yield strength of 60 ksi to identify the intersection points with increasing bar stress lines (see Figure 5.18). The critical embedment length and bond strength for both the mixtures (A4 and C3) are shown in Table 5.9. Again, A4 and C3 have comparable bond properties.

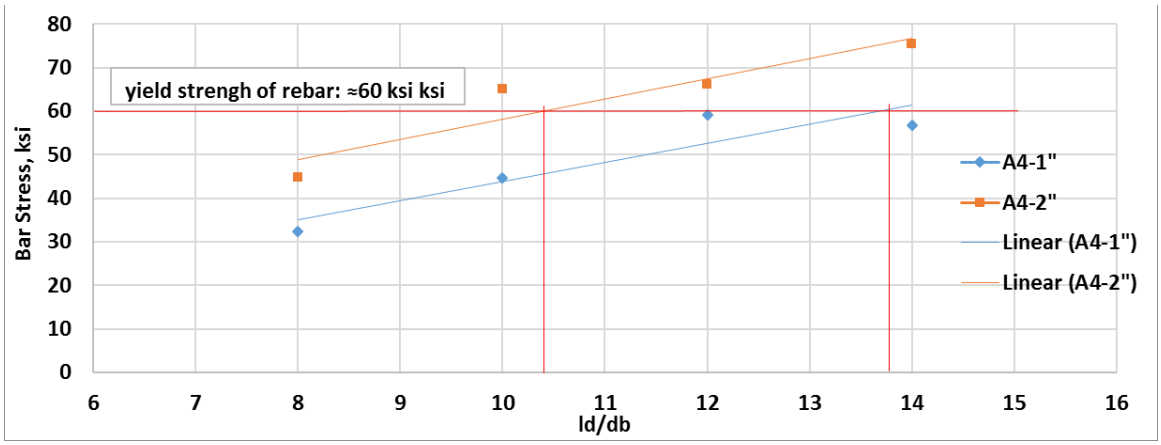

(a) UHPC mixture A4

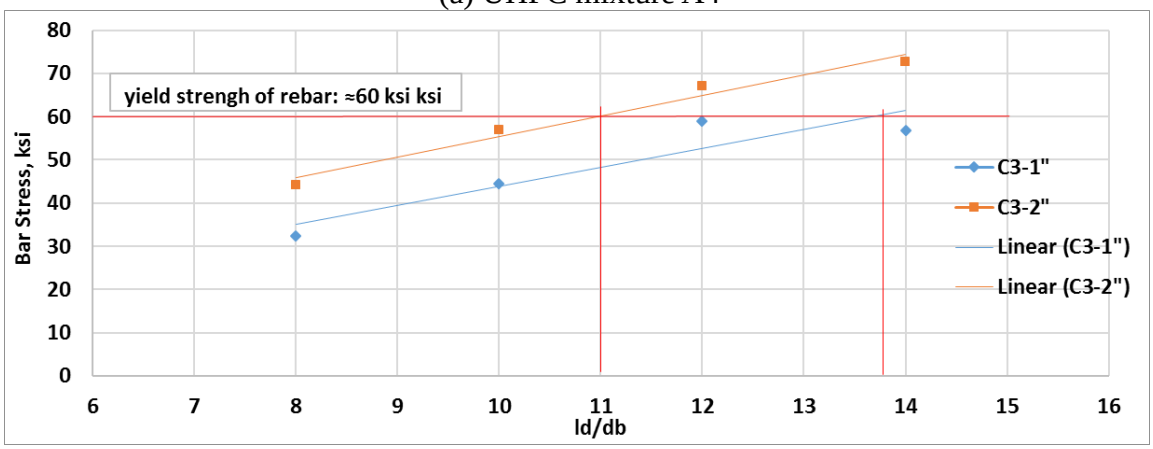

(b) UHPC mixture C3

Figure 5.18 Determination of critical embedment length

Table 5.9 Critical embedment length and bond strength

Side cover	A4		C3	
	Critical embedment length, l_d/d_b(in.)	Bond strength, ksi	Critical embedment length, l_d/d_b(in.)	Bond strength, ksi
1”	13.8 (9.0)	1.089	13.8 (9.0)	1.093
2”	10.6 (6.6)	1.384	11.0 (6.9)	1.374

5.2.2 Modes of failure

In general, bond can be considered as a combined behavior of three different mechanisms: mechanical anchorage between the ribs of reinforcing bar and surrounding contact surface of UHPC, friction force, and chemical adhesion. For deformed reinforcing bar used in this study, the anchorage plays the dominant role and resists most of the stress.

As shown in Figure 5.19a, for majority of tests, the bond failure occurred in the form of splitting cracking, some diagonal cracks formed but sometimes could not be visually observed. In addition, due to the bond forces radiated into the surrounding concrete, it commonly formed some conical cracks (Figure 5.19b) and spalling of concrete cover at some inclination from the rebar (approximately 40° was found in this study, Figure 5.19c); however, it still eventually failed with splitting cracks. This phenomenon was more clearly observed in the testing with larger bar stress, and it could be explained that the higher tensile stresses were generated, diagonal cracks occurred once exceeded the tensile strength of UHPC before splitting cracks. In some other cases, the specimens with the largest embedment length, the yielding failure of reinforcing bar occurred instead of failure due to splitting of UHPC. This is because the bond stress exceeded the yield stress of the bar (Figure 5.19d).

(a) Splitting cracking and diagonal cracks

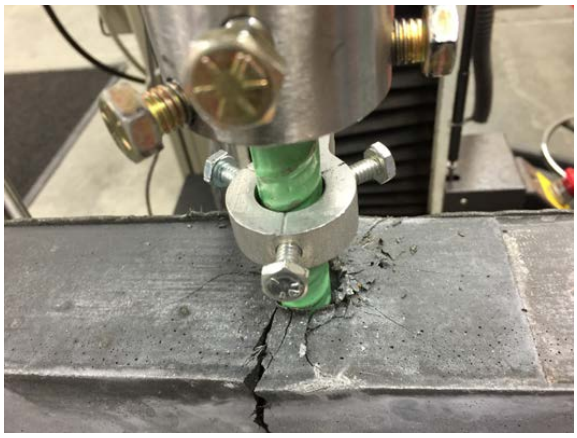

(b) Conical cracks

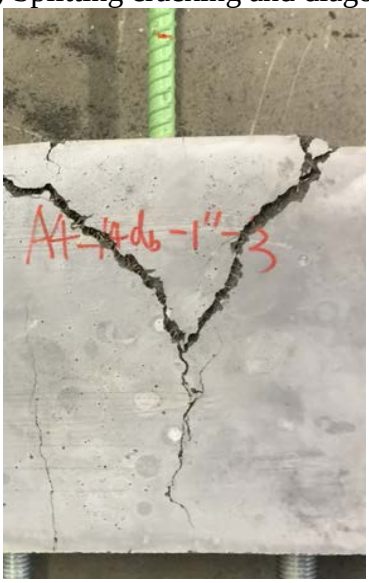

(c) Diagonal cracks and splitting cracking

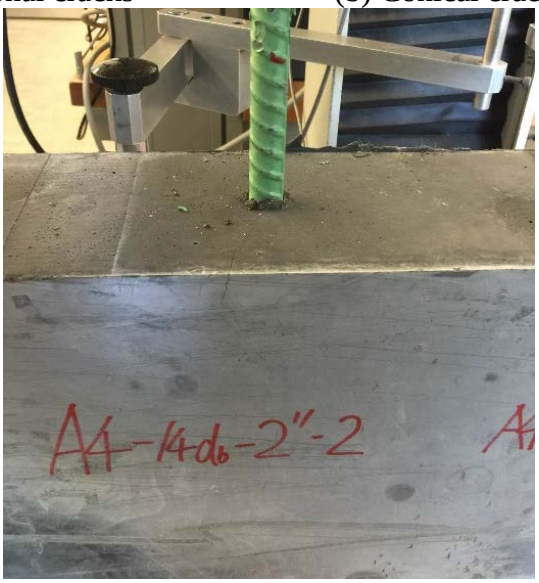

(d) Bar yielding

Figure 5.19 Some typical failure patterns

5.2.3 Load-slip relationship

Afefy and EI-Tony (2015) proposed an idealized bond-slip relationship curve of pull-out tests for the steel reinforcing bar in normal concrete, as shown in Figure 5.20, which is similar to the results of UPHC. The relationship curve is divided into four phases. Phase I shows the linear phase where almost no slip forms and chemical adhesion and static friction resist the axial stress. Phase II represents the non-linear progression of the curve, and it starts after the chemical adhesion yields, mechanical interlock between the ribs of reinforcing bar and surrounding contact surface of concrete begins to act as leading role

while dynamic frictional force plays a supporting role. In this phase, tiny splitting cracks, conical cracks and diagonal cracks form as the stress in concrete exceeds the tensile strength. The mechanical interlock keeps hardening with the increasing bar force and more visible cracks are formed until bond failures. Phase III is the residual phase (softening phase) that mechanical interlocking cannot resist applied load any more, and it shows the rapid reduction of load with significant increase in slip and widen cracks. In Phase IV, after fully cracking of concrete, some friction force still exists until eventually pull-off of reinforcing bar.

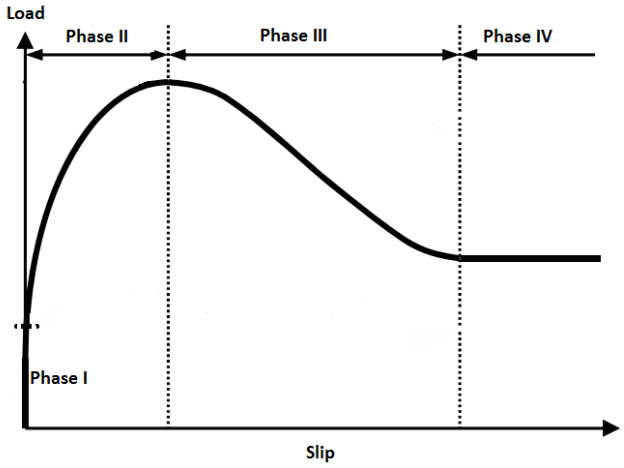

Figure 5.20 Idealized bond-slip relationship curve of pull-out tests (Afefy and EI-Tony 2015)

The load-slip relationship curves of all pull-out tests for the reinforcing bars in UHPC are plotted in Figures 5.21 and 5.22. In a few minor cases, the No. 8 anchoring bar at the bottom of beams for the sake of connecting the specimens with testing machine was sometimes pulled out before the splitting cracking, resulting in a quite small peak load. When such unacceptable failure happened, the load-slip relationship curves were abandoned and only the validated curves is plotted. For the deepest embedment length, the machine stopped automatically when reaching its capacity (29 kips), and the reinforcing

bar yielded in this case and no obvious cracks show on the surface of UHPC.

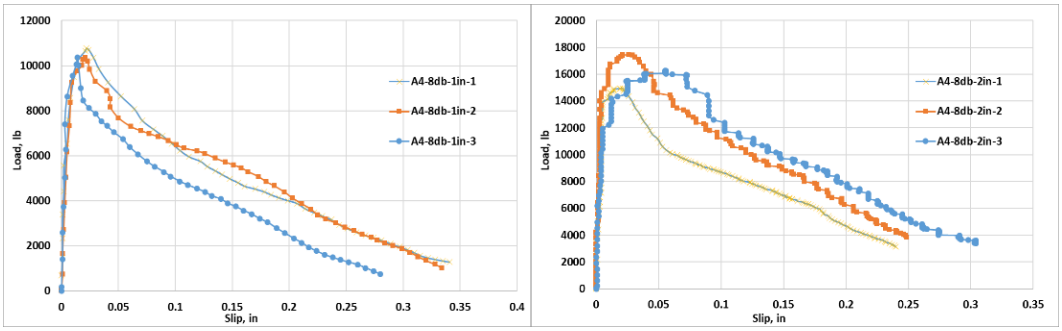

(a) A4-8d_b-1in.

(b) A4-8d_b-2in.

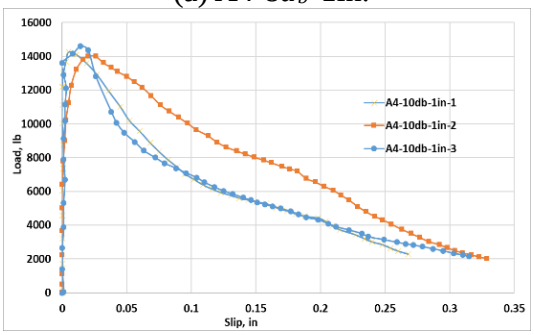

(c) A4-10d_b-1in.

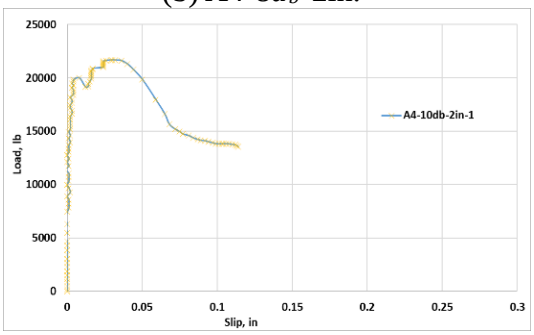

(d) A4-10d_b-2in.

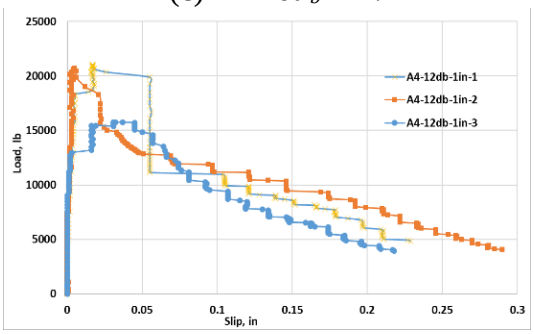

(e) A4-12d_b-1in.

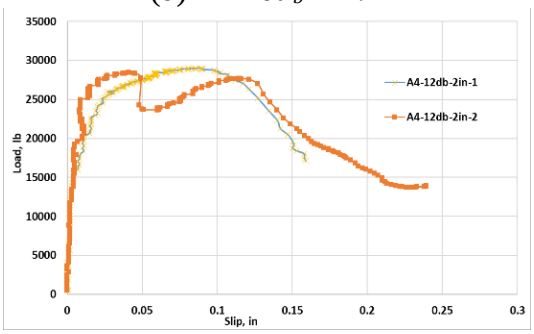

(f) A4-12d_b-2in.

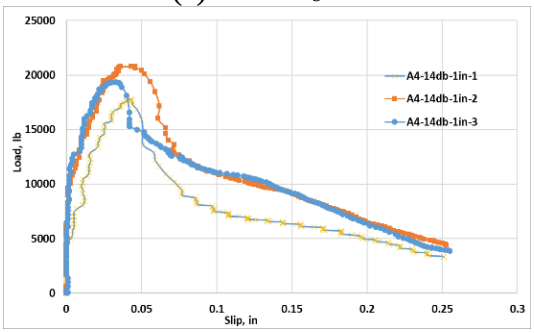

(g) A4-14d_b-1in.

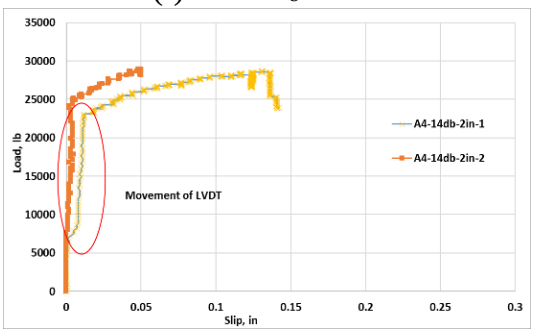

(h) A4-14d_b-2in.

Figure 5.21 Load-slip relationship curves of A4

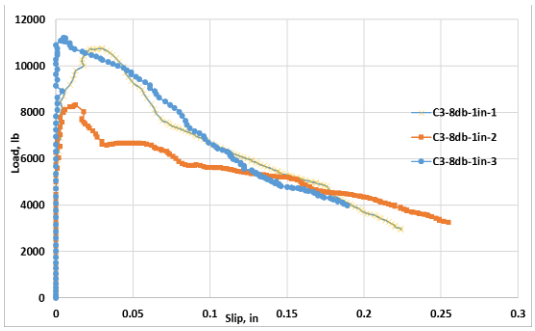

(a) C3-8d_b-1in.

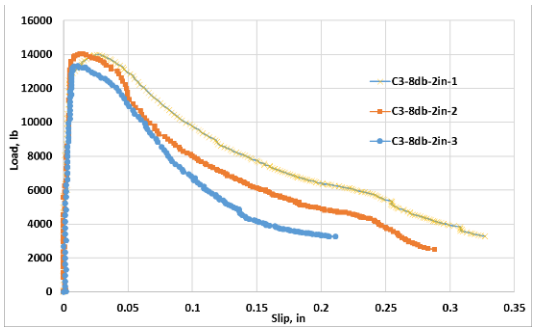

(b) C3-8d_b-2in.

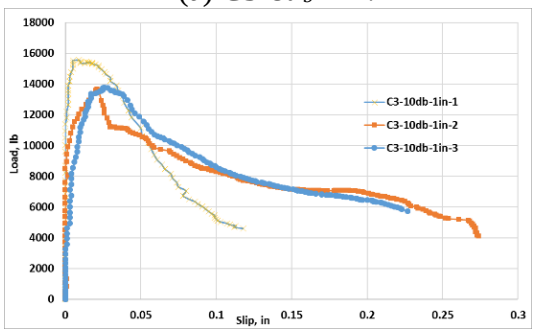

(c) C3-10d_b-1in.

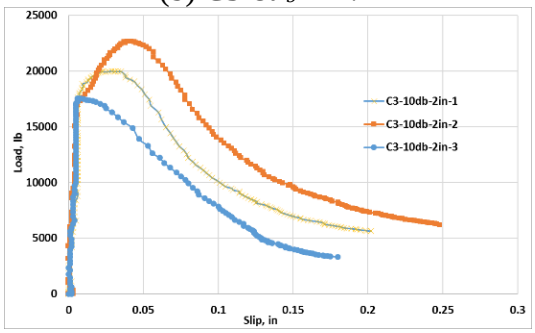

(d) C3-10d_b-2in.

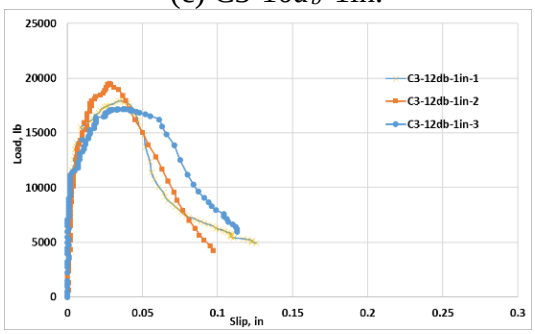

(e) C3-12d_b-1in.

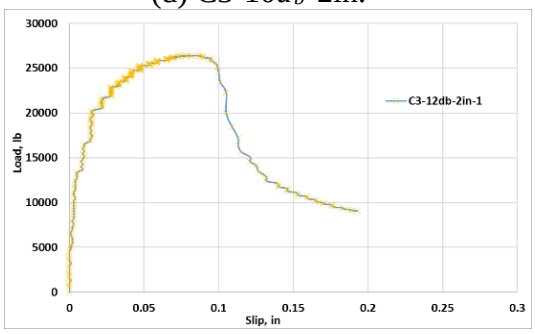

(f) C3-12d_b-2in.

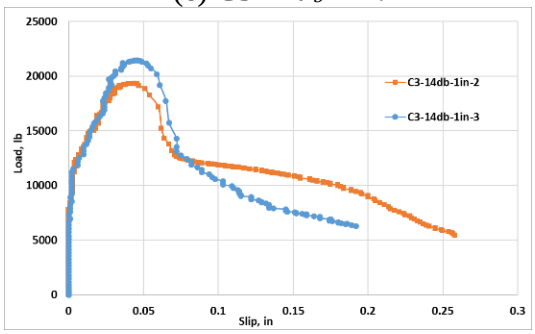

(g) C3-14d_b-1in.

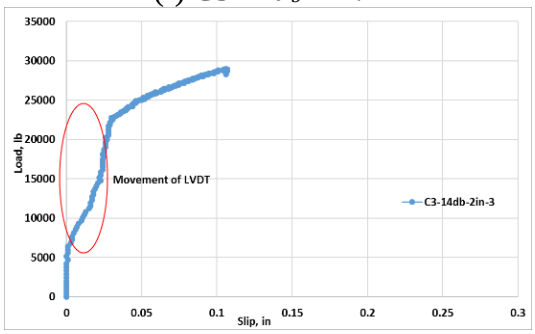

(h) C3-14d_b-2in.

Figure 5.22 Load-slip relationship curves of C3

As shown in Figures 5.21 and 5.22, the load-slip curves are greatly consistent with the idealized bond-slip relationship in Figure 5.20. Both the embedment length and side cover of rebar influence the bond behavior in UHPC. Besides, some other parameters, such as

bar size, bar type, bar spacing, compressive strength of UHPC, and content of steel fibers in UHPC, etc., are necessary to be evaluated in further study.

The embedment length has significant effect on the slip duration and bond performance in all the phases as exhibited in Figures 5.21 and 5.22. In the linear phase I, increase of the bar force was induced but almost no slip was observed. However, in some cases, slip was observed probably due to movement of LVDT. The chemical adhesion and static friction provided the axial force before mechanical interlock taking action can be assumed to be proportional with the embedment length; thus, the load at the first crack is linearly increased with increase in embedment length. In phase II, the mechanical interlock between the ribs of reinforcing bar and surrounding contact surface of concrete starts working. Longer the embedment length and more number of ribs results in longer duration of interlocking work and higher load carrying capacity. In Phase III and Phase IV after reaching the peak load, the load decreases drastically and slip takes place until rebar is fully pulled-out. Little difference is found in these two phases.

Side cover is another influencing factor evaluated in this study. By comparing Figures 5.21 and 5.22 where the only different design parameter is the side cover, the main differences are also found during the Phase I and Phase II. As expected, the maximum bar stress without the bar slip at Phase I increases with increased side cover. In Phase II, the mechanical interlock mechanism works for longer duration at the same loading rate, leading to a higher peak load. Again, no clear relationship is concluded due to limited side covers provided.

Chapter 6 CONCLUSIONS AND RECOMMENDATIONS

6.1 Summary and Conclusions

In this study, development of UHPC mixes with local materials for bridge joint connection applications is conducted. A comprehensive review of the existing study on UHPC is first reviewed. Twelve UHPC mixtures were developed using locally available materials, from which two viable UHPC mixtures (i.e., A4 and C3) are selected for further evaluation based on their flowability. The mechanical properties of two selected UHPC mixtures and their bond properties with the epoxy-coated reinforcing bars are investigated, from which one final UHPC mix design (C3) is recommended for application in the joint connections of intended bridge deck bulb tees.

Based on the experimental evaluation of UHPC mixtures, the following finding/conclusions can be drawn.

2) Based on the extended literature review and available UHPC mixtures, the locally available sand, cement and admixtures as well as domestic steel fibers are identified to produce the UHPC for intended bridge joint connection application. More importantly, the expensive materials, such as quartz powder and imported fibers, commonly used in the commercial products and other studies, are not used. Based on the workability (flow) test, two mix designs (A4 and C3) with adequate workability are selected for further experimental evaluation.

3) The proper mixing procedures of UHPC with local materials are recommended, and the aim is to achieve adequate workability of mixes with the thorough mixing time, based on the power and volume of mixer.

4) Following the standard test procedures for concrete and cementitious material characterization, the test methods for both the fresh and harden properties of UHPC are selected, and the pull-out strength tests of concrete are adopted for characterization of bond strength of reinforcing bars in UHPC. The tensile strength-related properties and tests of UHPC are emphasized.

5) The standard test method for flow of hydraulic cement mortar (ASTM C1437) (the flow test) is considered to evaluate the workability of UHPC. The flow tests of 12 preliminary UHPC mixtures are performed, and two viable UHPC mix designs (i.e., designated as A4 and C3 mix designs in this study) achieved the minimum required spread of 9.0 in. are selected for further experimental evaluation.

6) The compressive strength of UHPC is evaluated using 2 inch and 4 inch cube specimens (ASTM C109), respectively, as well as 4 x 8 inch cylinders. The 2 inch cubes exhibited greater compressive strength than the 4 inch cubes and 4 x 8 inch cylinders. The compressive strengths of specimens produced from C3 mixture are marginally greater than those produced from A4 mixture. It also shows that the compressive strength almost gains the full strength after 14 days.

7) The flexural strength (modulus of rupture) (ASTM C78), splitting tensile strength (ASTM C496), and the direct tension tests are conducted to evaluate the tensile strength associated properties. The direct tension test produced lowest tensile strength values, followed by the splitting tensile strength test and then the flexural strength test. The direct tension test using the dog bone-shape samples is regarded as the most accurate method to obtain the tensile strength properties. More than 80% of the full tensile strength is achieved after 7 days, and the tensile strength of the specimens produced from C3 mixture is about

30.8% higher than those produced from A4 mixture. Besides obtaining the tensile strength of the materials, the direct tension test is also capable of measuring the tensile stress-strain behavior of the specimens, from which the ductility of UHPC is characterized.

8) Both the autogenous and free shrinkage properties are measured using two different sizes (i.e., 4 x 4 x 11.25 inch vs. 1 x 1 x 11.25 inch) of specimens (ASTM C157). The small prism samples show significantly larger values of shrinkage than those of the large prism samples. Based on the results measured from the large prism samples, both the A4 and C3 mixtures have comparably same autogenous and free shrinkages, while the C3 mixture shows a smaller restrained shrinkage than that of A4 mixture based on the strain reading from the ring tests.

9) The freeze-thaw durability of UHPC is excellent when compared with normal concrete. The dynamic modulus based on hammer impact test increases instead of decreasing even after 600 conditioning cycles, the surface scaling due to frost action is also negligible.

10) The pull-out test is conducted to evaluate the bond strength of epoxy-coated reinforcing steel bar in UHPC, and the side cover and embedment length are investigated, with a No. 5 epoxy-coated rebar of Grade 60 and a given bar spacing of 7 inch. The majority of the pull-out specimens fail in splitting. For the bar with a longer embedment length, the yielding of the bar is observed. The A4 and C3 mixes result in comparably the same bond strength.

In summary, the mix design of UHPC with locally available materials and related mechanical properties tests are conducted. Based on the comparisons of material properties and bond strength of two selected mixes (i.e., A4 and C3), the C3 mixture exhibits better

mechanical performance than A4 mix, and it is thus recommended to use in the second phase of the project that involves structural testing and evaluation at the University of Washington.

6.2 Recommendations

The results of this study are limited to the mix designs and test methods used to develop the local material-produced UHPC for intended bridge joint connection application. Based on the mixture development and experimental program conducted in this study, the following recommendations are suggested to further improve UHPC mixtures and better understand the performance of UHPC:

6.2.1 Mixture design

1) In the present study, sand is sieved through ASTM No. 30 and No. 200 sieves to obtain the particle size range between 75-600 microns. Since the scalping of sand is extremely time and labor consuming, studies need to be conducted to understand the effect of nominal maximum size of particle on rheological, physical, and mechanical properties of UHPC.

2) Optimization of particle packing density is important to achieve greater mechanical strength of UHPC. Studies to determine particle packing of granular mixture that can help achieve workable mixes and superior mechanical behavior of UHPC need to be conducted.

3) Two water/cementitious material ratios (0.21 for A4 and 0.18 for C4) of UHPC are used in this study. However, it is possible to produce UHPC mixtures with w/cm ratio lower than 0.14. UHPC mixtures developed in this study should be further optimized with w/cm ratio lower than 0.14. UHPC mixtures produced with much lower w/cm ratios are expected to exhibit greater mechanical strength and superior durability characteristics.

4) In the present study, high levels of cement and silica fume contents are used. Further studies are needed to find the ways to replace cement and silica fume with greater replacements levels using GGBFS and fly ash. Thus, UHPC can be economical and eco-friendly.

6.2.2 Mechanical properties

1) The compressive strength, tensile strength and durability are directly dependent on curing and post setting heat treatment methods. Further study is recommended to investigate the effect of different curing regimens on the properties of UHPC and identify a practically feasible curing regimen.

2) Although it was established that UHPC exhibits superior resistance to rapid freeze-thaw resistance, freeze-thaw behavior of UHPC when exposed harsh environments and cold climates, such as marine environment, chlorine deicer coupled with freeze-thaw cycles, magnesium deicer coupled with freeze-thaw cycles, etc., should be investigated.

3) Both early-age and long-term shrinkage and creep performance due to loss of moisture and the shrinkage cracking tendency on the concrete surface with a risk of decreasing the quality and durability need to be completely understood as UHPC has a very low water/cementitious materials ratio. In addition, potential mitigation strategies, such as using shrinkage reducing admixtures (SRA), expansive cementitious materials, internal curing, etc., can be proposed to reduce the shrinkage cracking tendency.

4) In this study, due to the short gage length of extensometer, some cracks occur out of its range of gage length of measurement in the direct tension test. A modified setup (e.g., using the extensometer with a longer gage length) is needed to capture the ductile post-cracking behavior of UHPC in direct tension test.

5) Extensive study of pull-out (bond strength) tests regarding more design parameters (e.g., bar spacing, bar size, bar types, etc.), loading regimes (e.g., biaxial loading, triaxial loading, etc.), age of UHPC, etc., are recommended to fully understand the bond behaviors.

6) Other behaviors of UHPC when subjected to fatigue and dynamic impact loadings need to be evaluated to make it as a stronger contender for structural applications.

REFERENCES

AASHTO T334-08 (2012) “Standard Method of Test for Estimating the Cracking Tendency of Concrete”, American Association of State Highway and Transportation Officials, Washington, DC.

ACI committee 318-14. (2014) “Building Code Requirements for Structural Concrete and Commentary.” American Concrete Institute, Farmington Hills, Michigan.

ACI committee 408R-03. (2003, Reapproved 2012) “Bond and Development of Straight Reinforcing Bars in Tension.” American Concrete Institute, Farmington Hills, Michigan.

Afefy H. M. and El-Tony E. M. (2015) “Bond Behavior of Embedded Reinforcing Steel Bars for Varying Levels of Transversal Pressure.” Journal of Performance of Constructed Facilities, 30(2), pp. 1-10.

Ahlborn, T. M., Harris D., Misson D., et al. (2008) “Durability and Strength Characterization of Ultra-High Performance Concrete under Variable Curing Regimes”, Ultra High Performance Concrete (UHPC), Proceedings of the Second International Symposium on Ultra High Performance Concrete, Kassel, Germany, pp. 197-204.

Ahlborn, T. M., Harris D., Misson D., et al. (2011) “Characterization of Strength and Durability of Ultra-High-Performance Concrete Under Variable Curing Conditions”, Transportation Research Record: Journal of the Transportation Research Board, 2251, pp. 68-75.

Allena, S., and Newtson, C. M. (2011) “Ultra-High Strength Concrete Mixtures Using Local Materials”, Journal of Civil Engineering and Architecture, 5(4), pp. 322-330.

ASTM A820/A820M-15 (2015) “Standard Specification for Steel Fibers for Fiber-Reinforced Concrete, ASTM International”, West Conshohocken, PA.

ASTM C1018-97 (Withdrawn 2006) “Standard Test Method for Flexural Toughness and First-Crack Strength of Fiber-Reinforced Concrete (Using Beam with Third-Point Loading)”, ASTM International, West Conshohocken, PA.

ASTM C109/C109M-16a (2016) “Standard Test Method for Compressive Strength of Hydraulic Cement Mortars (Using 2-in. or [50-mm] Cube Specimens)”, ASTM International, West Conshohocken, PA.

ASTM C1202-12 (2012) “Standard Test Method for Electrical Indication of Concrete's Ability to Resist Chloride Ion Penetration”, ASTM International, West Conshohocken, PA.

ASTM C1231/C1231M-15 (2015) “Standard Practice for Use of Unbonded Caps in Determination of Compressive Strength of Hardened Cylindrical Concrete Specimens”, ASTM International, West Conshohocken, PA.

ASTM C128-15 (2015) “Standard Test Method for Relative Density (Specific Gravity) and Absorption of Fine Aggregate”, ASTM International, West Conshohocken, PA.

ASTM C136/C136M-14 (2014) “Standard Test Method for Sieve Analysis of Fine and Coarse Aggregates, ASTM International”, West Conshohocken, PA.

ASTM C1437-15 (2015) “Standard Test Method for Flow of Hydraulic Cement Mortar”, ASTM International, West Conshohocken, PA.

ASTM C157/C157M-08 (2014) “Standard Test Method for Length Change of Hardened Hydraulic-Cement Mortar and Concrete”, ASTM International, West Conshohocken, PA.

ASTM C192/C192M-16 (2016) “Standard Practice for Making and Curing Concrete Test Specimens in the Laboratory”, ASTM International, West Conshohocken, PA.

ASTM C39/C39M-16 (2016) “Standard Test Method for Compressive Strength of Cylindrical Concrete Specimens”, ASTM International, West Conshohocken, PA.

ASTM C469/C469M-14 (2014) “Standard Test Method for Static Modulus of Elasticity and Poisson’s Ratio of Concrete in Compression”, ASTM International, West Conshohocken, PA.

ASTM C496/C496M-11 (2004) “Standard Test Method for Splitting Tensile Strength of Cylindrical Concrete Specimens”, ASTM International, West Conshohocken, PA.

ASTM C617/C617M-15. (2015) “Standard Practice for Capping Cylindrical Concrete Specimens”, ASTM International, West Conshohocken, PA.

ASTM C666/C666M-15 (2015) “Standard Test Method for Resistance of Concrete to Rapid Freezing and Thawing”, ASTM International, West Conshohocken, PA.

ASTM C78/C78M-15b (2016) “Standard Test Method for Flexural Strength of Concrete (Using Simple Beam with Third-Point Loading)”, ASTM International, West Conshohocken, PA.

Aziz Omer Q. and Ahmed Ghafur H. (2012) “Mechanical Properties of Ultra-High Performance Concrete (UHPC)”. Twelfth International Conference on Recent Advances in Concrete Technology and Sustainability Issues, pp. 331-346.

Brain K., Brant P., Dean B., et al. (2007) “Design of Buchanan County, Iowa, Bridge Using Ultra High Performance Concrete and PI Girders”. Proceedings of the 2007 Mid-Continent Transportation Research Symposium, Ames, Iowa.

Collepardi, S., Coppola, L., Troli, R., tet al. (1997) “Mechanical Properties of Modified Reactive Powder Concrete”. Proceedings of the Fifth CANMET/ACI International Conference on Superplasticizers and Other Chemical Admixtures in Concrete, Rome, Italy, Publication No. SP-173, Ed., Malhotra V.M., American Concrete Institute, Farmington Hills, MI, pp. 1-21.

Cornelia Magureanu et al. (2012) “Mechanical Properties and Durability of Ultra-High-Performance Concrete”. ACI Materials Journal, 109(2), pp. 177-184.

Eppers, S., and Muller, C. (2008) “Autogeneous Shrinkage Strain of Ultra-High-Performance Concrete (UHPC)”. Ultra High Performance Concrete (UHPC), Proceedings of the Second International Symposium on Ultra High Performance Concrete, Kassel, Germany, pp. 433-441.

Glaubitt, André, and Bernhard Middendorf. “Non-destructive ultrasonic testing methods for quality control of UHPC”. Ultra High Performance Concrete (UHPC), Proceedings of the Second International Symposium on Ultra High Performance Concrete, Kassel, Germany, pp. 319-326.

Graybeal, B. A., and Hartmann, J. L. (2003) “Strength and Durability of Ultra-High Performance Concrete”. Concrete Bridge Conference, pp. 1-20.

Graybeal B. A. (2006) “Material Property Characterization of Ultra-High Performance Concrete”. US Department of Transportation, Federal Highway Administration. Publication No. FHWA-HRT-06-103.

Graybeal, B. A. (2007) “Compressive Behaviour of Ultra-High_Performance Riber-Reinforced Concrete”. ACI Materials Journal, 104(2), pp. 146-152.

Graybeal B. A. (2010) “Behavior of Ultra-High Performance Concrete Connections Between Precast Bridge Deck Elements”. Proceedings of the Concrete Bridge Conference, Phoenix, Arizona.

Graybeal Benjamin A. (2012) “Construction of Field-Cast Ultra-High Performance Concrete Connections”. US Department of Transportation, Federal Highway Administration. Publication No: FHWA-HRT-12-038.

Graybeal, B. A., and Baby, F. (2013) “Development of Direct Tension Test Method for Ultra-High-Performance Fiber-Reinforced Concrete”. ACI Materials Journal, 110(2), pp. 177-186.

Graybeal, B. A. (2015) “Compression Testing of Ultra-High-Performance Concrete”. Advances in Civil Engineering Materials, 4(2), pp. 102-112.

Hassan A.M.T. and Jones S.W. (2012) “Non-destructive testing of ultra-high performance fibre reinforced concrete (UHPFRC): A feasibility study for using ultrasonic and resonant frequency testing techniques”. Construction and Building Materials, 35, pp. 361-367.

Hansen L.P. and Jensen B.C (1999) “A New Building System Using Joints of Ultra High-Strength Fibre Reinforced Concrete”. Innovation in Concrete Structures: Design and Construction: Proceedings of the International Conference on Creating with Concrete, University of Dundee, Scotland, pp. 543-552.

Ioan Sosa and Cornelia Magureanu (2010) “Shrinkage of Ultra High Performance Concrete”. Acta Technica Napocensis: Civil Engineering and Architecture, 53, pp. 32-37.

Karmout, M. (2009) “Mechanical Properties of Ultra High Performance Concrete produced in Gaza Strip”. Master Thesis, Islamic University of Gaza.

Kusumawardaningsinh, Y., Fehling, E., and Ismail, M. (2015a). “UHPC compressive strength test specimens: Cylinder or cube?” Procedia Engineering, 125, pp. 1076-1080.

Kusumawardaningsih, Y., Fehling, E., Ismail, M., et al. (2015b) “Tensile strength behavior of UHPC and UHPFRC”. Procedia Engineering, 125, pp. 1081-1086.

Lawend K. Askar, Bassam A. Tayeh and B.H. Abu Bakar (2013) “Effect of Different Curing Conditions on the Mechanical Properties of UHPFC” Iranica Journal of Energy and Environment, 4 {(3) Geo-hazards and Civil Engineering}, pp. 299-303.

Liu J., Han F., Cui G., et al. (2016) “Combined effect of coarse aggregate and fiber on tensile behavior of ultra-high performance concrete”. Construction and Building Materials, 121, pp. 310-318.

Neville, A. M. (1996) “Properties of Concrete (4th Edition)”. New York: John Wiley & Sons, Inc.

Nguyen D. L., Ryu G. S., Koh K. T., et al. (2001) “Size and geometry dependent tensile behavior of ultra-high-performance fiber-reinforced concrete”. Composites: Part B, 58, pp. 279-292.

Orgass, M. and Klug, Y. (2004) “Fibre Reinforced Ultra-High Strength Concretes”. Proceedings of the International Symposium on Ultra High Performance Concrete, Kassel University Press, Kassel, Germany, pp. 637-647.

Palecki, S., and Seizer, M. J. (2008). “Ultra-High-Performance concrete under frost and de-icing salt attack”. Ultra High Performance Concrete (UHPC), Proceedings of the Second International Symposium on Ultra High Performance Concrete, Kassel, Germany, pp. 443-451.

Park S. H., Kim D. J., Ryu G. S. Koh K. T. (2012) “Tensile behavior of Ultra High Performance Hybrid Fiber Reinforced Concrete”. Cement and Concrete Composites, 34, pp. 184.

Perry V.H and Zakariasen D. (2004) “First Use of Ultra-High Performance Concrete for an Innovative Train Station Canopy” Portland cement Association, Concrete Technology Today CT042, 25(2), pp. 1-2.

Pyo S., Wille K., El-Tawil S., et al. (2015) “Strain rate dependent properties of ultra-high performance fiber reinforced concrete (UHP-FRC) under tension”. Cement and Concrete Composites, 56, pp. 15-24.

Richard, P., and Cheyrezy, M. (1995) “Composition of reactive powder concretes”. Cement and Concrete Research, 25, pp. 1501-1511.

Reda M. M., Shrive N. G., and Gillott J. E. (1999) “Microstructural investigation of innovative UHPC”. Cement and Concrete Research, 29, pp. 323-329.

RILEM Technical Committees RILEM TC 162-TDF. (2001) “Test and Design Methods for Steel Fibre Reinforced Concrete - Recommendations: Uni-axial Tension Test for Steel Fibre Reinforced Concrete”. Materials and Structures, 34(1), pp. 3-6.

Russel, H. G., and Graybeal, B. A. (2013) “Ultra-High Performance Concrete: A State-of-the-Art Report for the Bridge Community”. US Department of Transportation, Federal Highway Administration Publication No. FHWA-HRT-13-060.

Shetty M.S. (2005) “Concrete Technology - Theory and Practice” S. Chand & Company Ltd., New Delhi, India.

Sobuz H. R., Ali M.S. Mohamed, Singh M., Griffith M.C., and Sheikh A.H. (2016)

"Manufacturing ultra-high performance concrete utilising conventional materials and production methods". Construction and Building Materials, 111, pp. 251-261.

Tran N. T., Tran T. K., and Kim D. J. (2015) "High rate response of ultra-high performance fiber-reinforced concretes under direct tension". Cement and Concrete Research, 69, pp. 72-87.

USBR. (1992) "Procedure for Direct Tensile Strength, Static Modulus of Elasticity, and Poisson's Ratio of Cylindrical Concrete Specimens in Tension". In USBR 4914. United Stated Department of Interior, Bureau of Reclamation.

Victor Y. G., Lawrence F. K., and Imberly E. K. (2009) "Short-term Tensile Creep and Shrinkage of Ultra-High Performance Concrete". Cement and Concrete Composites, 31(3), pp. 147-152.

Wille K., and Boisvert-Cotulio C. (2015) "Material efficiency in the design of ultra-high performance concrete". Construction and Building Materials, 86, pp. 33-43.

Wille K., Kim D. J., Naaman A. E. (2011) "Strain-hardening UHP-FRC with low fiber contents". Materials and Structures, 44(3), pp. 583-598.

Wu Z., Shi C., and He W. (2017) "Comparative study on flexural properties of ultra-high performance concrete with supplementary cementitious materials under different curing regimes". Construction and Building Materials, 136, pp. 307-313.

Yuan, J., and Graybeal, B. A. (2014) "Bond Behavior of Reinforcing Steel in Ultra-High Performance Concrete". U.S. Department of Transportation, Federal Highway Administration. Publication No. FHWA-HRT-14-090.

Zhao S, Fan J., and Sun W. (2014) "Utilization of iron ore tailings as fine aggregate in ultra-high performance concrete". Construction and Building Materials, 50, pp. 540-548.

Americans with Disabilities Act (ADA) Information:
This material can be made available in an alternate format by emailing the Office of Equal Opportunity at wsdotada@wsdot.wa.gov or by calling toll free, 855-362-4ADA(4232). Persons who are deaf or hard of hearing may make a request by calling the Washington State Relay at 711.

Title VI Statement to Public:
It is the Washington State Department of Transportation's (WSDOT) policy to assure that no person shall, on the grounds of race, color, national origin or sex, as provided by Title VI of the Civil Rights Act of 1964, be excluded from participation in, be denied the benefits of, or be otherwise discriminated against under any of its federally funded programs and activities. Any person who believes his/her Title VI protection has been violated, may file a complaint with WSDOT's Office of Equal Opportunity (OEO). For additional information regarding Title VI complaint procedures and/or information regarding our non-discrimination obligations, please contact OEO's Title VI Coordinator at (360) 705-7082.